

# 1 Extreme heterogeneity of influenza 2 virus infection in single cells

3 Alistair B. Russell<sup>1</sup>, Cole Trapnell<sup>2</sup>, Jesse D. Bloom<sup>1,2\*</sup>

\*For correspondence:  
jbloom@fredhutch.org

4 <sup>1</sup>Basic Sciences Division and Computational Biology Program, Fred Hutchinson Cancer  
5 Research Center, Seattle, United States; <sup>2</sup>Department of Genome Sciences, University of  
6 Washington, Seattle, United States

7

8 **Abstract** Viral infection can dramatically alter a cell's transcriptome. However, these changes  
9 have mostly been studied by bulk measurements on many cells. Here we use single-cell mRNA  
10 sequencing to examine the transcriptional consequences of influenza virus infection. We find  
11 extremely wide cell-to-cell variation in the productivity of viral transcription – viral transcripts  
12 comprise less than a percent of total mRNA in many infected cells, but a few cells derive over half  
13 their mRNA from virus. Some infected cells fail to express at least one viral gene, but this gene  
14 absence only partially explains variation in viral transcriptional load. Despite variation in viral load,  
15 the relative abundances of viral mRNAs are fairly consistent across infected cells. Activation of  
16 innate immune pathways is rare, but some cellular genes co-vary in abundance with the amount of  
17 viral mRNA. Overall, our results highlight the complexity of viral infection at the level of single cells.

18

## 19 Introduction

20 Viruses can cause massive and rapid changes in a cell's transcriptome as they churn out viral mRNAs  
21 and hijack cellular machinery. For instance, cells infected with influenza virus at high multiplicity  
22 of infection (MOI) express an average of 50,000 to 100,000 viral mRNAs per cell, corresponding  
23 to 5 to 25% of all cellular mRNA (Hatada et al., 1989). Infection can also trigger innate-immune  
24 sensors that induce the expression of cellular anti-viral genes (Killip et al., 2015; Iwasaki and Pillai,  
25 2014; Crotta et al., 2013). This anti-viral response is another prominent transcriptional signature of  
26 high-MOI influenza virus infection in bulk cells (Geiss et al., 2002).

27 However, initiation of an actual influenza infection typically involves just a few virions infecting  
28 a few cells (Varble et al., 2014; Poon et al., 2016; Leonard et al., 2017; McCrone et al., 2017). The  
29 dynamics of viral infection in these individual cells may not mirror bulk measurements made  
30 on many cells infected at high MOI. Over 70 years ago, Max Delbrück showed that there was a  
31 ~100-fold range in the number of progeny virions produced per cell by clonal bacteria infected  
32 with clonal bacteriophage (Delbrück, 1945). Subsequent work has shown similar heterogeneity  
33 during infection with other viruses (Zhu et al., 2009; Schulte and Andino, 2014; Combe et al., 2015;  
34 Akpinar et al., 2016), including influenza virus (Heldt et al., 2015).

35 In the case of influenza virus infection, targeted measurements of specific proteins or RNAs  
36 have shed light on some factors that contribute to cell-to-cell heterogeneity. The influenza virus  
37 genome consists of eight negative-sense RNA segments, and many infected cells fail to express  
38 one more of these RNAs (Heldt et al., 2015; Dou et al., 2017) or their encoded proteins (Brooke  
39 et al., 2013). In addition, activation of innate-immune responses is inherently stochastic (Shalek  
40 et al., 2013, 2014; Bhushal et al., 2017; Hagai et al., 2017), and only some influenza-infected cells  
41 express anti-viral interferon genes (Perez-Cidoncha et al., 2014; Killip et al., 2017). However, the  
42 extent of cell-to-cell variation in these and other host and viral factors remains unclear, as does the

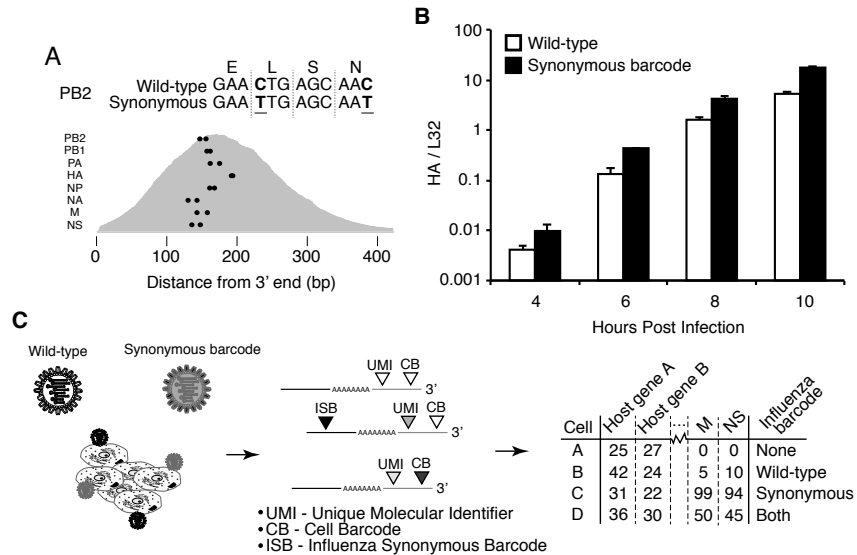


**Figure 1.** Experimental design. **(A)** We engineered a virus that carried two synonymous mutations near the 3' end of each mRNA. At top are the mutations for PB2. At bottom are locations of the synonymous mutations relative to the typical distribution of read depth for our 3'-end sequencing. **(B)** The wild-type and synonymously barcoded viruses transcribe their genes with similar kinetics. The abundance of the viral hemagglutinin (HA) transcript relative to the cellular housekeeping gene L32 was assessed by qPCR in A549 cells infected at an MOI of 0.5 (as determined on MDCK-SIAT1 cells). Error bars  $\pm$  S.D., n=3. **(C)** For the single-cell mRNA sequencing, A549 cells were infected with an equal mixture of wild-type and synonymously barcoded virus. Immediately prior to collection, cells were physically separated into droplets and cDNA libraries were generated containing the indicated barcodes. The libraries were deep sequenced, and the data processed to create a matrix that gives the number of molecules of each transcript observed in each cell. Infected cells were further annotated by whether their viral mRNAs derived from wild-type virus, synonymously barcoded virus, or both.

**Figure 1-source data 1.** Sequences of wild-type and barcoded viruses are in [viralsequences.fasta](#).

43 association among them in individual infected cells.

44 Here we use single-cell mRNA sequencing to quantify the levels of all cellular and viral mRNAs  
45 in cells infected with influenza virus at low MOI. We find extremely large variation in the amount  
46 of viral mRNA expressed in individual cells. Both co-infection and activation of innate-immune  
47 pathways are rare in our low-MOI infections, and do not appear to be the major drivers of cell-  
48 to-cell heterogeneity in viral transcriptional load. Individual infected cells often fail to express  
49 specific viral genes, and such gene absence explains some but certainly not all of the cell-to-cell  
50 heterogeneity. A variety of cellular genes, including ones involved in the oxidative-stress response,  
51 co-vary with viral transcriptional load. Overall, our work demonstrates remarkable heterogeneity in  
52 the transcriptional outcome of influenza virus infection among nominally identical cells infected  
53 with a relatively pure population of virions.

## 54 Results

### 55 Strategy to measure mRNA in single virus-infected cells.

56 We performed single-cell mRNA sequencing using a droplet-based system that physically isolates  
57 individual cells prior to reverse transcription ([Zheng et al., 2017; Macosko et al., 2015; Klein et al., 2015](#)).  
58 Each droplet contains primers with a unique *cell barcode* that tags all mRNAs from that  
59 droplet during reverse-transcription. Each primer also contains a *unique molecular identifier (UMI)*  
60 that is appended to each mRNA molecule during reverse transcription. The 3' ends of the mRNAs are  
61 sequenced and mapped to the human and influenza virus transcriptomes to determine transcript  
62 identities. This information is combined with that provided by the UMIs and cell barcodes to

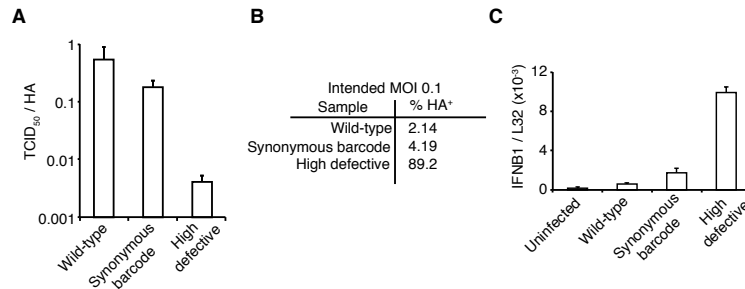


**Figure 2.** The viral stocks in our experiments are relatively pure of defective particles. **(A)** Our viral stocks have a higher ratio of infectious particles to HA virion RNA compared to a high-defective stock propagated at high MOI. HA viral RNA was quantified by qPCR on virions. Error bars  $\pm$  S.D., n=6 (qPCR replicates). **(B)** Our viral stocks have a higher ratio of infectious particles to particles capable of expressing HA protein. A549 cells were infected at an MOI of 0.1, and the percentage of cells expressing HA protein at 9 hours post-infection was quantified by antibody staining and flow cytometry. **(C)** Our viral stocks are less immunostimulatory than virus propagated at high MOI when used at the same number of infectious units as calculated by TCID<sub>50</sub>. Note that this fact does not necessarily imply that they are more immunostimulatory per virion, as the high-MOI stocks also have more virions per infectious unit as shown in the first two panels. Measurements of *IFNB1* transcript by qPCR normalized to the housekeeping gene L32 in A549 cells at 10 hours post infection at an MOI of 0.5. Error bars  $\pm$  S.D., n=3. Note that MOIs were calculated by TCID<sub>50</sub> on MDCK-SIAT1 cells, whereas the experiments in this figure involved infection of A549 cells.

**Figure 2–Figure supplement 1.** Full flow cytometry data for panel B .

63 quantify the number of molecules of each mRNA species that have been captured for each cell.  
 64 Infected cells will express viral as well as cellular mRNAs – however the cell barcodes and  
 65 UMIs cannot distinguish whether a cell was initially infected by one or multiple viral particles. We  
 66 therefore engineered an influenza virus (strain A/WSN/1933) that additionally carried *viral barcodes*  
 67 consisting of synonymous mutations near the 3' end of each transcript (**Figure 1A**). Critically, these  
 68 synonymous mutations did not greatly impact viral growth kinetics (**Figure 1B**). We infected A549  
 69 human lung carcinoma cells with an equal mix of the wild-type and synonymously barcoded  
 70 viruses. Cells infected by a single virion will exclusively express mRNAs from either wild-type or  
 71 synonymously barcoded virus, whereas cells that are co-infected with multiple virions will often  
 72 express mRNAs from both the wild-type and synonymously barcoded viruses (**Figure 1C**).

73 We took care to generate stocks of virus that were relatively “pure” of defective particles. Stocks  
 74 of viruses typically contain an array of biologically active viral particles, some of which are defective  
 75 for replication owing to mutations or deletions in essential viral genes (*von Magnus, 1954; Huang*  
*et al., 1970; Brooke, 2014; Fonville et al., 2015; Lauing and Andino, 2010; Dimmock et al., 2014;*  
*Saira et al., 2013*). These defective particles become prevalent when a virus is grown at high MOI,  
 76 where complementation permits the growth of otherwise deleterious genotypes. To minimize the  
 77 levels of defective particles, we propagated our viral stocks at low MOI for a relatively brief period of  
 78 time (*Xue et al., 2016*). We validated that our stocks exhibited greater purity of infectious particles  
 79 than a stock propagated at high MOI by verifying that they had a higher ratio of infectious particles  
 80 to virion RNA (**Figure 2A**) and to particles capable of inducing expression of a single viral protein  
 81 (**Figure 2B**). In addition, viral stocks with many defective particles are more immunostimulatory  
 82 per infectious unit (e.g., TCID<sub>50</sub>) than low-defective stocks (*Tapia et al., 2013; Lopez, 2014*), in part  
 83 simply because there are more physical virions per infectious unit (**Figure 2A,B**). We confirmed that  
 84 our viral stocks induced less interferon per infectious unit than a stock propagated at higher MOI  
 85 (**Figure 2C**).

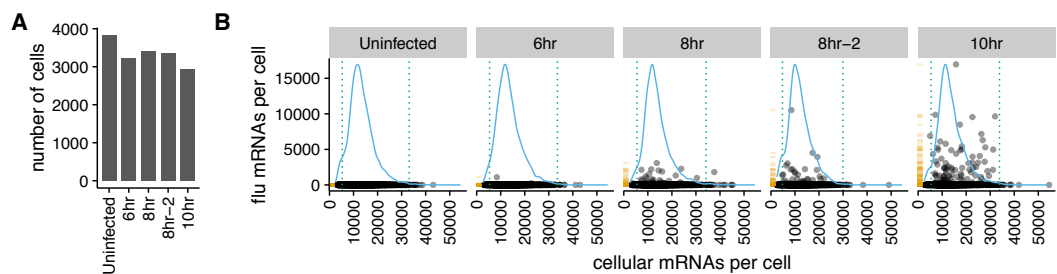


**Figure 3.** There is a very wide distribution in the amount of viral mRNA per cell. **(A)** Number of cells sequenced for each sample. **(B)** The number of cellular and viral mRNAs detected for each cell is plotted as a point. The blue lines show the overall distribution of the number of cellular mRNAs per cell. The orange rug plot at the left of each panel shows the distribution of the number of viral mRNAs per cell. Cells outside the dotted green lines were considered outliers with suspiciously low or high amounts of cellular mRNA (possibly derived from two cells per droplet), and were excluded from all subsequent analyses. *Figure 3–Figure Supplement 1* shows the exact distributions of the fraction of viral mRNA per cell.

**Figure 3–Figure supplement 1.** Cumulative fraction plot of proportion of total mRNA from virus.

### 88 Single cells show an extremely wide range of expression of viral mRNA.

89 We infected A549 cells at low MOI with a mixture of the wild-type and synonymously barcoded  
90 viruses, and collected cells for sequencing at 6, 8, and 10 hours post-infection, performing two  
91 slightly different variants of the experiment for the 8-hour timepoint. For most of the samples, we  
92 replaced the infection inoculum with fresh media at one-hour post-infection, thereby ensuring that  
93 most infection was initiated during a narrow time window. However, for the second 8-hour sample  
94 (which we denote as “8hr-2” in the figures), we did *not* perform this media change and instead left  
95 the cells in the original infection inoculum. The rationale for including a sample without a media  
96 change was to determine the importance of synchronicity of the timing of infection as discussed  
97 later in this subsection.

98 We recovered between 3,000 and 4,000 cells for each sample (*Figure 3A*). As expected for a low-  
99 MOI infection, most cells expressed little or no viral mRNA (*Figure 3B*, *Figure 3–Figure Supplement 1*).  
100 Also as expected, the amount of viral mRNA per cell among infected cells increased over time  
101 (*Figure 3B*, *Figure 3–Figure Supplement 1*). But what was most notable was how widely the number  
102 of viral mRNA molecules varied among infected cells. While the fraction of mRNA derived from  
103 virus was <0.1% for most cells, viral mRNA constituted half the transcriptome in a few cells at 8 and  
104 10 hours (*Figure 3B*, *Figure 3–Figure Supplement 1*).

105 A complicating factor is that uninfected cells could have small amounts of viral mRNA due  
106 to leakage of transcripts from lysed cells. It is therefore important to establish a threshold for  
107 identifying truly infected cells. We can do this by taking advantage of the fact that roughly half the  
108 infecting virions bear synonymous barcodes. Reads derived from lysed cells will be drawn from  
109 both wild-type and synonymously barcoded viral transcripts. However, most cells are infected by at  
110 most one virion, and so the reads from truly infected cells will usually derive almost entirely from  
111 one of the two viral variants. *Figure 4A* shows the fraction of viral reads in individual cells from each  
112 viral variant, and *Figure 4B* indicates the fraction of viral reads from the most abundant variant in  
113 that cell. Most cells with large amounts of viral mRNA have viral transcripts exclusively derived from  
114 one viral variant – indicating non-random partitioning as expected from viral infection. However,  
115 cells with a small amount of viral mRNA often have viral transcripts from both variants, as expected  
116 from the random partitioning associated with simple mRNA leakage. Finally, a few cells with large  
117 amounts of viral mRNA have viral transcripts from both variants, likely reflecting co-infection.

118 We determined the threshold amount of viral mRNA per cell for each sample at which the  
119 barcode partitioning clearly resulted from infection rather than leakage (*Figure 4C*, *Figure 4–Figure  
120 Supplement 2*), and used these thresholds to annotate cells that we were confident were truly  
121 infected. We also annotated as co-infected cells above this threshold that had mRNA from both

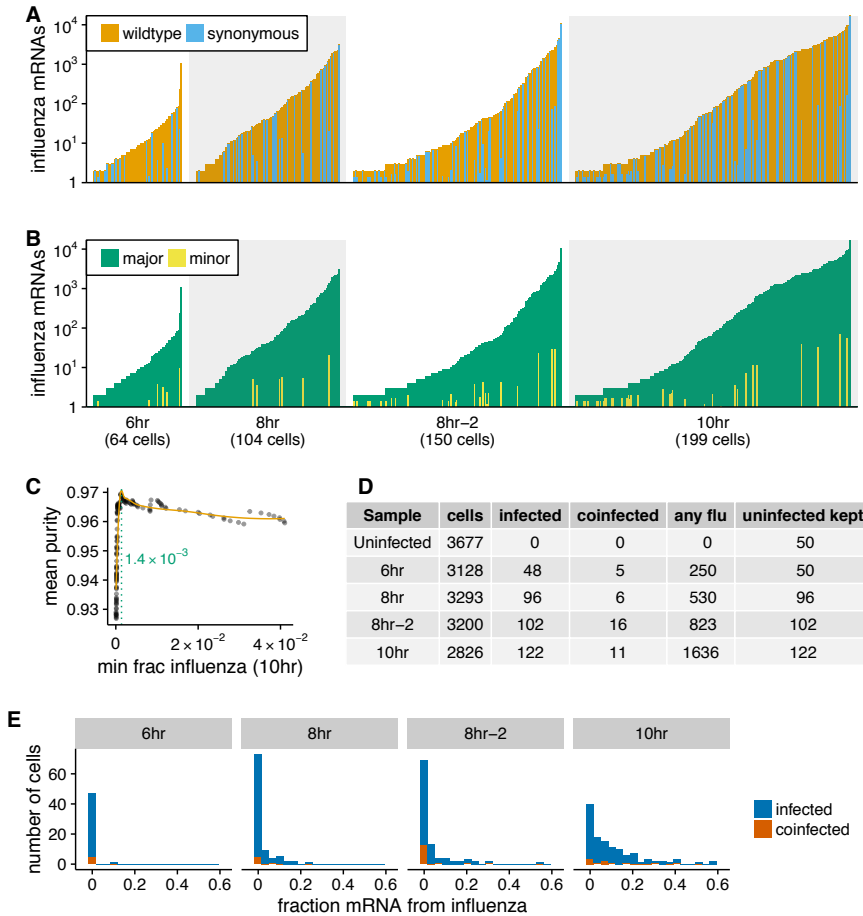


**Figure 4.** Synonymous barcodes on the viral mRNAs distinguish true infections from cells that contain viral mRNAs derived from leakage of lysed cells. **(A)** Cells with at least two viral mRNAs for which the barcode could be called, arranged in order of increasing influenza transcript counts. Bar heights denote the number viral mRNAs on a  $\log_{10}$  scale, bar coloring is linearly proportional to the fractions of viral mRNAs derived from wild-type and synonymously barcoded virus. **(B)** Same as (A), but each bar is colored according to the relative fraction of the more common (major) and less common (minor) virus variant. At low levels of viral mRNA there is often a roughly equal mix, suggesting contamination with viral mRNAs leaked from lysed cells. At higher levels of viral mRNA, cells generally have only one viral variant, suggesting infection initiated by a single virion. A few cells are also obviously co-infected with both viral variants. **(C)** We determined a threshold for calling “true” infections by finding the amount of viral mRNA per cell at which the viral barcode purity no longer increases with more viral mRNA. The purity is the fraction of all viral mRNA in a cell derived from the most abundant viral barcode in that cell. We fit a curve (orange line) to the mean purity of all cells with more than the indicated amount of viral mRNA, and drew the cutoff (dotted green line) at the point where this curve stopped increasing with the fraction of total mRNA derived from virus. This plot illustrates the process for the 10-hour sample, see **Figure 4–Figure Supplement 2** for similar plots for other samples. See the Methods for details. **(D)** The number of cells identified as infected and co-infected for each sample, as well as the number of cells with any viral read. For all subsequent analyses, we subsampled the number of uninfected cells per sample to the greater of 50 or the number of infected cells. **(E)** Distribution of the fraction of mRNA per cell derived from virus for both infected and co-infected cells. **Figure 4–Figure Supplement 3** shows these same data in a cumulative fraction plots and calculates Gini coefficients to quantify the heterogeneity in viral mRNA load.

**Figure 4–Figure supplement 1.** Number of viral barcodes called.

**Figure 4–Figure supplement 2.** Thresholds for calling infected cells.

**Figure 4–Figure supplement 3.** Cumulative distributions of viral mRNA per cell and Gini coefficients.

**Figure 4–Figure supplement 4.** Synchronization of infection does not greatly affect heterogeneity.

**Figure 4–Figure supplement 5.** Effects of infectious dose or coinfection state.

122 viral variants. **Figure 4D** shows the number of cells annotated as infected and co-infected for each  
 123 sample – these cells are just a small fraction of the number of cells with any viral read. These  
 124 annotation thresholds are conservative, and may miss some true low-level infections. However, it is  
 125 important that the analyses below are restricted to cells that are truly infected with virus, so we  
 126 accepted the possible loss of some low-level infections in order to avoid false positives. In addition,  
 127 the synonymous viral barcodes only identify co-infections by viruses with different barcodes – since  
 128 the barcodes are at roughly equal proportion, we expect to miss about half of the co-infections.  
 129 Since we annotate about ~10% of the infected cells as co-infected by viruses with different barcodes  
 130 (**Figure 4D**), we expect another ~10% of the infected cells to also be co-infected but not annotated  
 131 as so by our approach. Because most cells are not infected, we subsampled the uninfected cells to  
 132 the numbers shown in **Figure 4D** to balance the proportions of infected and uninfected cells for all  
 133 subsequent analyses.

134 Strikingly, the extreme variation in the number of viral transcripts per cell remains even after we  
 135 apply these rigorous criteria for annotating infected cells (**Figure 4E**). The fraction of viral mRNA per  
 136 infected cell follows a roughly exponential distribution, with many cells having few viral transcripts  
 137 and a few cells having many. At 6 and 8 hours <10% of infected cells are responsible for over half  
 138 the viral transcripts, while at 10 hours <15% of infected cells produce over half the viral transcripts  
 139 (**Figure 4–Figure Supplement 3**). One way to quantify the heterogeneity of a distribution is to  
 140 calculate the Gini coefficient (**Gini, 1921**), which ranges from 0 for a completely uniform distribution,  
 141 to 1 for a maximally skewed distribution. **Figure 4–Figure Supplement 3** shows the Gini coefficients  
 142 for the distribution of viral mRNA across infected cells for each sample. The Gini coefficients  
 143 are  $\geq 0.64$  for all samples. As a fun point of comparison, these Gini coefficients indicate that the  
 144 distribution of viral mRNA across infected cells is more uneven than the distribution of income in  
 145 the United States (**Alvaredo, 2011**).

146 One possible source of heterogeneity in the amount of viral mRNA per cell is variability in the  
 147 timing of infection. If some cells are infected earlier in the experiment than others, then they  
 148 might have substantially more viral mRNA. However, several lines of evidence indicate that this  
 149 is not the major cause of heterogeneity across cells. First, the sample for which the infection  
 150 inoculum was never removed (8hr-2) only shows slightly more heterogeneity than samples for  
 151 which the inoculum was washed away after one hour (**Figure 4E, Figure 4–Figure Supplement 3**),  
 152 despite the fact that the potential time window for infection is much longer in the former sample.  
 153 Second, in an independent experiment, we performed completely synchronized infections by  
 154 pre-binding virus to cells on ice and then washing away unbound virus before bringing the cells  
 155 to 37°C (**Dapat et al., 2014**). As shown in **Figure 4–Figure Supplement 4**, flow cytometry staining  
 156 found that the heterogeneity in the levels of individual viral proteins was not markedly different  
 157 for these synchronized infections than in the absence of pre-binding and washing. Finally, viral  
 158 mRNA expression from the secondary spread of virus from infected cells does not appreciably occur  
 159 during the timeframes of our experiments, since **Figure 4B** does not show the pervasive presence  
 160 of mixed barcodes that would occur in this case. Therefore, variability in the timing of infection is  
 161 not the dominant cause of the cell-to-cell heterogeneity in our experiments.

162 Notably, **Figure 4E** shows that there are co-infected cells with both low and high amounts of  
 163 viral mRNA, suggesting that the initial infectious dose does not drive a simple continuous increase  
 164 in viral transcript production. In support of this view, we used flow cytometry to quantify the levels  
 165 of individual viral proteins in cells infected at various MOIs or for which we could delineate co-  
 166 infection status (**Figure 4–Figure Supplement 5**). This analysis shows that sub-populations of cells  
 167 that express similarly low and high levels of viral proteins persist across a wide range of infectious  
 168 doses, although co-infection can influence the relative proportion of infected cells that fall into  
 169 these sub-populations (**Figure 4–Figure Supplement 5**).

170 **Absence of viral genes partially explains cell-to-cell variability in viral load.**

171 The influenza genome is segmented, and cells can fail to express a viral mRNA if the encoding  
 172 gene segment is not packaged in the infecting virion or fails to initiate transcription after infection.  
 173 Indeed, several groups have reported that the majority of infected cells fail to express at least  
 174 one viral gene (*Brooke et al., 2013; Heldt et al., 2015; Dou et al., 2017*). We wondered if the  
 175 absence of specific viral genes might be associated with reduced amounts of viral mRNA within  
 176 single infected cells. In particular, transcription of influenza virus mRNAs is performed by the viral  
 177 ribonucleoprotein (RNP) complex, which consists of the three proteins that encode the tripartite  
 178 polymerase (PB2, PB1, and PA) as well as nucleoprotein (NP) (*Huang et al., 1990*). Each viral gene  
 179 segment is associated with one RNP in incoming infecting virions, but secondary transcription by  
 180 newly synthesized RNPs requires the presence of the viral genes encoding each of the four RNP  
 181 proteins (*Vreede et al., 2004; Eisfeld et al., 2015*). This secondary transcription is a major source  
 182 of viral mRNAs, as evidenced by the fact that blocking synthesis of the RNP proteins reduces the  
 183 amount of viral mRNA by several orders of magnitude in bulk cells (*Figure 5-Figure Supplement 1*).

184 We examined the total amount of viral mRNA versus the expression of the genes from each  
 185 viral segment (*Figure 5A, Figure 5-Figure Supplement 2, Figure 5-Figure Supplement 3*). Note  
 186 that influenza virus expresses ten major gene transcripts from its eight gene segments, as the  
 187 M and NS segments are alternatively spliced to produce the M1 / M2 and NS1 / NEP transcript,  
 188 respectively (*Dubois et al., 2014*). However, an inherent limitation of current established single-cell  
 189 mRNA sequencing techniques is that they only sequence the 3' end of the transcript (*Zheng et al.,  
 190 2017; Macosko et al., 2015; Klein et al., 2015; Cao et al., 2017*). Since the alternative spliceforms  
 191 M1 / M2 and NS1 / NEP share the same 3' ends, we cannot distinguish them and therefore will refer  
 192 simply to the combined counts of transcripts from each of these alternatively spliced segments as  
 193 the M and NS genes.

194 Cells that lack an RNP gene never derive more than a few percent of their mRNAs from virus, con-  
 195 firming the expected result that all four RNP genes are essential for high levels of viral transcription  
 196 (*Figure 5A, Figure 5-Figure Supplement 2, Figure 5-Figure Supplement 3*). However, we observe  
 197 cells that lack each of the other non-RNP genes but still derive  $\approx 40\%$  of their mRNAs from virus,  
 198 suggesting that none of the other genes are important for high levels of viral transcription. These  
 199 results are statistically supported by *Figure 5B*, which shows that absence of any RNP gene but *not*  
 200 any other viral gene is associated with reduced amounts of viral mRNA. However, gene absence  
 201 clearly does not explain all of the variability in viral gene expression, since even cells expressing all  
 202 viral genes exhibit a very wide distribution in the amount of viral mRNA that they express. Specifi-  
 203 cally, at both 8 and 10 hours, the amount of viral mRNA in individual cells expressing all eight viral  
 204 genes still ranges from <1% to >50% (*Figure 5A, Figure 5-Figure Supplement 2, Figure 5-Figure  
 205 Supplement 3*). Furthermore, the actual distribution of viral mRNA per infected cell (*Figure 4E*) does  
 206 not match the mostly bi-modal shape expected under a simple model where RNP gene absence  
 207 and Poisson co-infection are the only factors (*Figure 5-source data 2*), indicating that there are  
 208 additional sources of variability beyond whether cells have full complement of RNP genes.

209 We also quantified the fraction of infected cells that completely failed to express a given gene. We  
 210 limited this analysis to examining the presence / absence of the non-RNP genes in cells expressing  
 211 all four RNP genes, since we might fail to detect viral transcripts that are actually present at low  
 212 levels in RNP-deficient cells due to the lower viral burden in these cells. At the 8- and 10-hour time  
 213 points, between 5% and 17% of cells fail to express any one of the four non-RNP genes (*Figure 5C,  
 214 Figure 5-source data 1*). The absence of a given gene appears to be an independent event, as the  
 215 probability of observing all four non-RNP genes in a cell is well predicted by simply multiplying  
 216 the probabilities of observing each gene individually (*Figure 5C and Figure 5-source data 1*). If we  
 217 extrapolate the frequencies at which cells lack non-RNP genes to the RNP genes, then we would  
 218 predict that 35-50% of infected cells express mRNAs from all eight genes. This estimate of the  
 219 frequency at which infected cells express mRNAs from all eight gene segments is slightly higher than

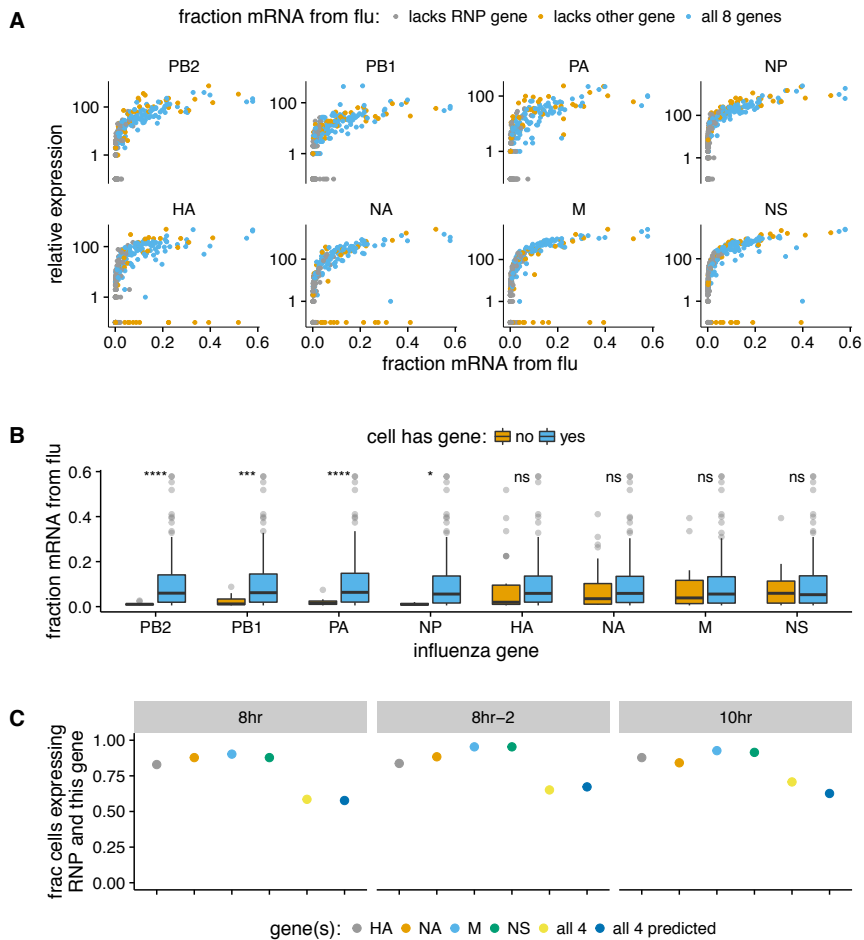


**Figure 5.** The absence of viral genes explains some of the variability in the amount of viral mRNA per cell. **(A)** The normalized expression of each viral gene as a function of the total fraction of mRNA in each infected cell derived from virus, taken over all time points. Cells with high viral burden always express all RNP genes, but some cells with high viral burden lack each of the other genes. Plots for individual samples are in *Figure 5-Figure Supplement 2*, and a plot that excludes known coinfecting cells is in *Figure 5-Figure Supplement 3*. **(B)** Box and whisker plots showing the per-cell viral burden among cells with >0.5% of their mRNA from virus, binned by whether or not the cells express each gene. A Wilcoxon signed-rank test was used to test the null hypothesis that absence of each gene does not affect viral burden: \*\*\*\* =  $P < 10^{-4}$ , \*\*\* =  $P < 10^{-3}$ , \* =  $P < 0.05$ , ns = not significant. The trends are similar if we look only at the 10-hour sample (*Figure 5-Figure Supplement 4*) or exclude known co-infected cells (*Figure 5-Figure Supplement 5*). **(C)** The fraction of cells that express each of the four other genes among cells that express all RNP genes, as well as the fraction that express *all* four of the other genes. The fraction that express *all* four genes is well predicted by simply multiplying the frequencies of cells that express each gene individually, indicating that gene absence is approximately independent across these genes.

**Figure 5-Figure supplement 1.** Secondary transcription is a major source of viral mRNA during bulk infections.

**Figure 5-Figure supplement 2.** Like panel (A), but shows samples individually.

**Figure 5-Figure supplement 3.** Like panel (A), but excludes coinfecting cells with mixed viral barcodes.

**Figure 5-Figure supplement 4.** Like panel (B) but for the 10-hr sample only.

**Figure 5-Figure supplement 5.** Like panel (B) but excludes coinfecting cells with mixed viral barcodes.

**Figure 5-source data 1.** The numerical data for panel (C) are in `p_missing_genes.csv`.

**Figure 5-source data 2.** Simulation with a simple model for the expected heterogeneity due to Poisson co-infection and presence / absence of the full RNP is in `simple_Poisson_model.html`.

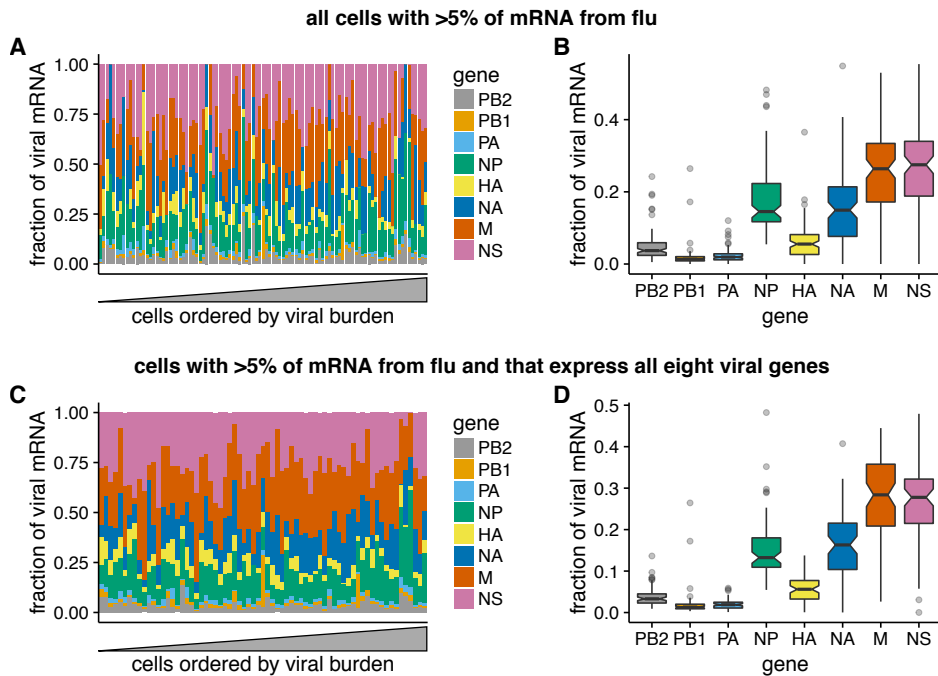


**Figure 6.** Relative expression of influenza virus genes in highly infected cells (>5% of total mRNA from virus). **(A)** The fraction of viral mRNA from each viral gene for each cell. **(B)** Box plots showing the distribution of the fraction of viral mRNA per cell from each viral gene. The black lines at the notches are the medians, and the tops and bottoms of boxes indicate the first and third quartiles. Whiskers extend to the highest or lowest data point observed within 1.5x the interquartile range, outliers shown as circles. Notches extend 1.58x the interquartile range divided by the square root of the number of observations. **(C), (D)** The same plots, but only including cells for which we observed at least one molecule of each viral gene.

**Figure 6-source data 1.** The raw data for all cells are in `p_flu_expr_all.csv`.

**Figure 6-source data 2.** The raw data for fully infected cells are in `p_flu_expr_fullyinfected.csv`.

220 previous estimates of 13% (*Brooke et al., 2013*) and 20% (*Dou et al., 2017*). At least one difference  
 221 is that *Brooke et al. (2013)* stained for proteins whereas we examined the expression of mRNAs – it  
 222 is likely that some cells contain mutated viral genes that fail to produce stable protein even when  
 223 mRNA is expressed.

#### 224 The relative amounts of different viral mRNAs are more consistent across cells.

225 The results above show that the amount of viral mRNA in infected cells varies over several orders  
 226 of magnitude. Does the relative expression of viral genes exhibit similar cell-to-cell variability?  
 227 To address this question, we focused on cells that derived >5% of their mRNA from virus, since  
 228 estimates of relative viral gene expression will be less noisy in cells with more viral mRNAs.

229 In contrast to the extreme variability in the total viral mRNA per cell, the fraction of this viral  
 230 mRNA derived from each gene is much more consistent across cells (**Figure 6A**). Total viral mRNA  
 231 varies by orders of magnitude, but the fraction from any given viral gene is fairly tightly clustered  
 232 around the median value for all cells (**Figure 6B**). The relative levels of each viral mRNA in our cells  
 233 are similar to prior bulk measurements made by Northern blots (*Hatada et al., 1989*), which also  
 234 found an expression hierarchy of M > NS ≫ NP > NA > HA ≫ PB2 ~ PB1 ~ PA. The cell-to-cell  
 235 consistency in the relative expression of different viral genes is even tighter if we limit the analysis  
 236 only to cells that express all eight viral genes (**Figure 6C,D**). Therefore, with the exception of complete  
 237 gene absence, the factors that drive the dramatic cell-to-cell variability in the amount of viral mRNA  
 238 have roughly similar effects on all viral genes in a given cell. This finding is consistent with prior  
 239 work showing positive correlations among the abundance of several viral genome segments in

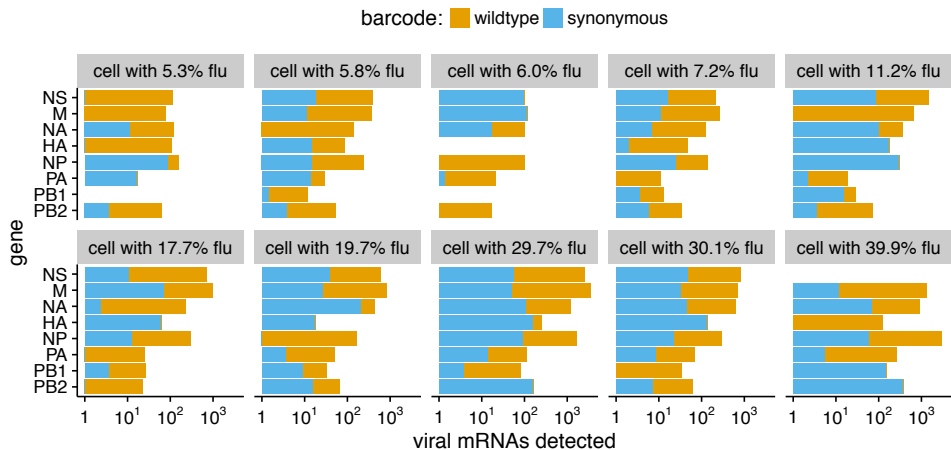


**Figure 7.** The abundance of each viral transcript in cells that are co-infected with the two viral variants and have >5% of their mRNA derived from virus. The bars show the logarithms of the numbers of each viral mRNA detected, and are colored in linear proportion to the fraction of that mRNAs derived from wild-type or synonymously barcoded virus.

**Figure 7-Figure supplement 1.** Co-infected cells express roughly equal amounts of a gene from each infecting viral variant.

**Figure 7-source data 1.** The raw data plotted in this figure are in `p_co-infection.csv`.

**Figure 7-source data 2.** The sequence of the HA viral RNA carrying the GFP gene is in `HAflank-eGFP.fasta`.

240 individual cells ([Heldt et al., 2015](#)).

#### 241 **Co-infection can provide infected cells with the full complement of viral genes.**

242 Our sequencing enables us to identify the rare cells that were co-infected with both wild-type and  
 243 synonymously barcoded viral variants. Overall, we captured 10 such co-infected cells that had >5%  
 244 of their mRNA derived from virus (**Figure 7**). Seven of these 10 cells expressed all eight viral genes.  
 245 The majority (4 of 7) of these cells would *not* have expressed all the viral genes in the absence  
 246 of co-infection, since they have at least one gene exclusively derived from each viral variant. For  
 247 instance, the cell with 11.2% of its mRNA from virus in the upper right of **Figure 7** expresses M only  
 248 from the wildtype viral variant, and NP and HA only from the synonymously barcoded variant. Our  
 249 data therefore provide the first direct single-cell observation of the fact that co-infection can rescue  
 250 missing viral genes ([Brooke et al., 2013, 2014; Fonville et al., 2015; Aguilera et al., 2017](#)).

251 Another observation from **Figure 7** is that co-infected cells usually express roughly equal  
 252 amounts of transcripts from each of the two viral variants. This observation is consistent with the  
 253 finding by [Dou et al. \(2017\)](#) and [Huang et al. \(2008\)](#) that the temporal window for co-infection is  
 254 short – if both viral variants infect a cell at about the same time, then neither will have a headstart  
 255 and so each will have a roughly equal opportunity to transcribe its genes.

256 To support this idea with a larger dataset albeit at lower resolution, we generated a virus in  
 257 which the HA coding sequence was replaced by GFP. We then co-infected cells with a mix of wildtype  
 258 and ΔHA-GFP virus and used flow cytometry to score cells for the presence of HA only (infection by  
 259 wildtype virus), GFP only (infection by ΔHA-GFP virus), or both (co-infection) as shown in **Figure 7-**  
**Figure Supplement 1.** As in our single-cell sequencing data, we found that expression of HA and GFP  
 260 were highly correlated, indicating that co-infected cells typically expressed roughly equal amounts  
 261 of transcript from each viral variant.

#### 263 **Activation of the interferon response is rare in single infected cells.**

264 Because our sequencing captured all polyadenylated transcripts, we can examine whether there  
 265 are prominent changes in the host-cell transcriptome in sub-populations of infected cells. Influenza

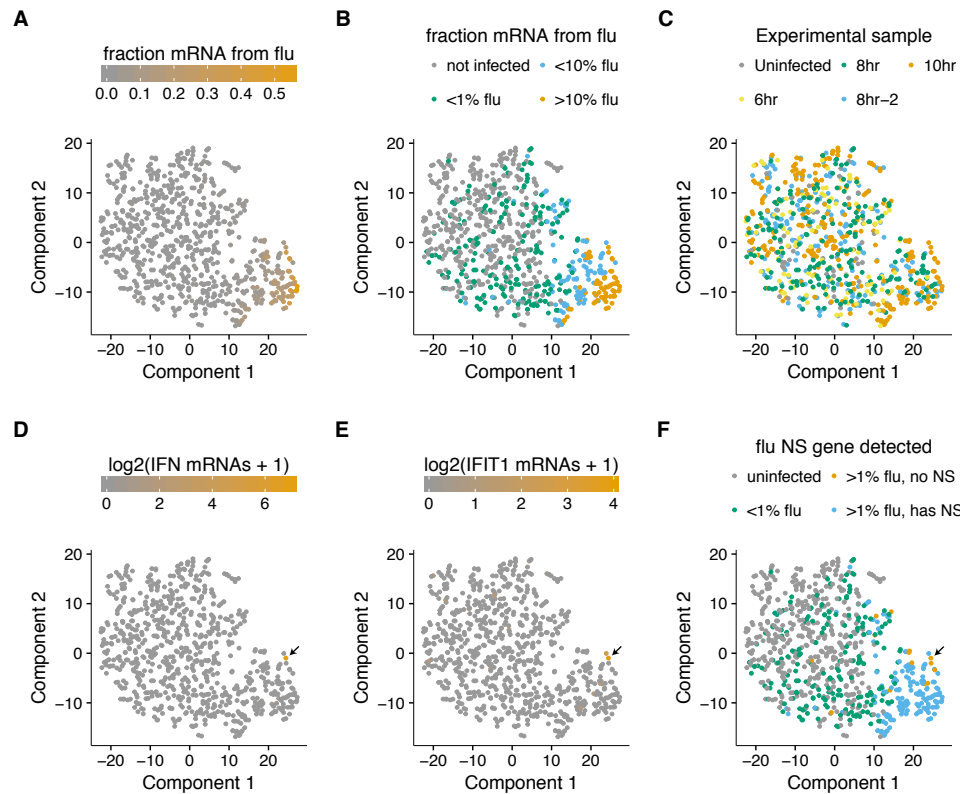


**Figure 8.** A t-SNE plot created by semi-supervised clustering using genes that co-vary with viral infection status. Each point is a single cell, and each panel shows an identical layout but colors the cells according to a different property. **(A), (B)** Cells colored by the fraction of their mRNA derived from virus. **(C)** Cells colored by the experimental sample. **(D)** Cells colored by the number of detected transcripts from type I and III interferons (IFN). Only one cell has detectable interferon expression (in orange, indicated with arrow). **(E)** Cells colored by the expression of the interferon-stimulated gene IFIT1. **(F)** Cells colored by whether they express the viral NS gene. The one interferon-positive cell is lacking NS, but so are many interferon-negative cells.

266 virus infection can trigger innate-immune sensors that lead to the transcriptional induction of  
 267 type I and III interferons, and subsequently of anti-viral interferon-stimulated genes (*Killip et al., 2015; Iwasaki and Pillai, 2014; Crotta et al., 2013*). However, activation of the interferon response  
 268 is stochastic and bi-modal at the level of single cells (*Chen et al., 2010; Shalek et al., 2013, 2014; Perez-Cidoncha et al., 2014; Bhushal et al., 2017; Hagai et al., 2017*). We therefore hypothesized  
 269 that we might see two sub-populations of infected cells: one in which the interferon response  
 270 inhibited viral transcription, and another in which the virus was able to express high levels of its  
 271 mRNA by evading or blocking this response.

272 To examine whether there were distinct sub-populations of virus-infected cells, we used a  
 273 semi-supervised t-SNE approach (*Van der Maaten and Hinton, 2008*) to cluster cells by genes that  
 274 co-varied with viral infection status. As shown in *Figure 8A,B*, this approach effectively grouped cells  
 275 by the amount of viral mRNA that they expressed. Sample-to-sample variation was regressed away  
 276 during the clustering, as cells did not obviously group by time-point, with expected exception that  
 277 the uninfected and 6-hour samples had few cells in the region of the plot corresponding to large  
 278 amounts of viral mRNA (*Figure 8C*).

279 But to our surprise, we did not see a prominent clustering of infected cells into sub-populations  
 280 as expected if the interferon response was strongly activated in some cells. To investigate fur-  
 281 ther, we annotated each cell by the total number of type I and III interferon transcripts detected.  
 282 Remarkably, only a single cell expressed detectable interferon (*Figure 8D*). We also examined

285 interferon-stimulated genes, which are induced by autocrine and paracrine interferon signaling.  
 286 **Figure 8E** shows expression of one such gene, IFIT1 (*Fensterl and Sen, 2011*). As with interferon  
 287 itself, expression of IFIT1 was rare and most prominent in the single interferon-positive cell, pre-  
 288 sumably due to the higher efficiency of autocrine versus paracrine signaling. Notably, interferon  
 289 and interferon-stimulated genes were also relatively ineffective at blocking viral transcription in the  
 290 single cell in which they were potently induced, since >10% of the mRNA in this cell was derived  
 291 from virus (**Figure 8A,B,D,E**).

292 We posited that the paucity of interferon induction might be due to the activity of influenza  
 293 virus's major interferon antagonist, the NS1 protein (*García-Sastre et al., 1998; Hale et al., 2008*).  
 294 We therefore identified cells that expressed substantial amounts of viral mRNA but lacked the  
 295 NS gene (**Figure 8F**). Consistent with the idea that NS1 is important for suppressing interferon,  
 296 the one interferon-positive cell lacked detectable expression of the NS gene. But other cells that  
 297 lacked NS expression still failed to induce a detectable interferon response, despite often having a  
 298 substantial amount of their mRNA derived from virus (**Figure 8**). This result is in line with other work  
 299 showing that NS1-deficient influenza virus does not deterministically induce interferon (*Killip et al.,  
 300 2017; Kallfass et al., 2013*). Therefore, many individual infected cells fail to activate innate-immune  
 301 responses even when the virus lacks its major interferon antagonist.

### 302 **Some host genes co-vary with viral gene expression.**

303 We examined whether any host genes were differentially expressed in cells with more viral mRNA.  
 304 We restricted this analysis to infected cells with all eight viral genes in order to focus on cellular  
 305 genes that were associated with viral mRNA burden independent of effects due to the presence  
 306 or absence of particular viral transcripts. We identified 43 cellular genes that co-varied with viral  
 307 mRNA expression at a false discovery rate of 0.1 (**Figure 9**, **Figure 9-source data 1**).

308 A gene-set analysis shows that many cellular genes that are associated with the amount of viral  
 309 mRNA are involved in the response to reactive oxygen species or hypoxia (**Figure 9-source data 2**).  
 310 Genes known or suspected to be regulated by the Nrf2 master regulator in response to oxidative  
 311 stress are often expressed at higher levels in cells with more viral mRNA (**Figure 9**). These genes  
 312 produce proteins that are involved in detoxification of reactive oxygen species or resultant products,  
 313 the management of misfolded proteins, the electron transport chain, or a general stress response  
 314 (**Figure 9-Figure Supplement 1**). We additionally see reduced expression of the nitric oxide synthase  
 315 interacting protein (NOSIP). Transient oxidative stress is known to occur during viral infection, and  
 316 may act in a proviral fashion via MAPK activation driving vRNP export (*Amatore et al., 2014*). The  
 317 antioxidant response is thought to be largely antiviral, potentially through inhibition of MAPK activity  
 318 (*Lin et al., 2016; Sgarbanti et al., 2014*). To directly test the effect of transient oxidative stress, we  
 319 compared the fraction of cells that expressed detectable viral protein when infected either with or  
 320 without pre-treatment to suppress oxidative stress. **Figure 9-Figure Supplement 2** shows that the  
 321 cells pre-treated with an antioxidant exhibited less frequent detectable expression of viral protein.  
 322 These results, in conjunction with the differential expression test in **Figure 9** and the prior work  
 323 mentioned above, suggest that oxidative stress acts in a proviral fashion.

324 The gene-set analysis also found that the amount of viral mRNA was associated with the  
 325 expression of genes involved in the G2-M cell-cycle checkpoint (**Figure 9-source data 2**). The cell-  
 326 cycle associated genes CCND3, MKI67, UBE2S, and CENPF are all expressed at significantly lower  
 327 levels in cells with more viral mRNA (**Figure 9**). However, our data are not sufficient to determine  
 328 whether the lower expression of these genes is a cause or effect of the reduction in viral mRNA.

329 Interestingly, none of the cellular genes that are significantly associated with the amount of viral  
 330 mRNA in our study are among the 128 genes that *Watanabe et al. (2010)* report as having been  
 331 identified multiple times in genome-wide screens for factors affecting influenza virus replication.  
 332 One possible explanation is that most of the cell-to-cell heterogeneity in our experiments might  
 333 arise from viral segment absence or mutations, pure stochasticity, or more subtle alterations in  
 334 host-cell state – not due to changes in expression of the type of single large-effect genes that are

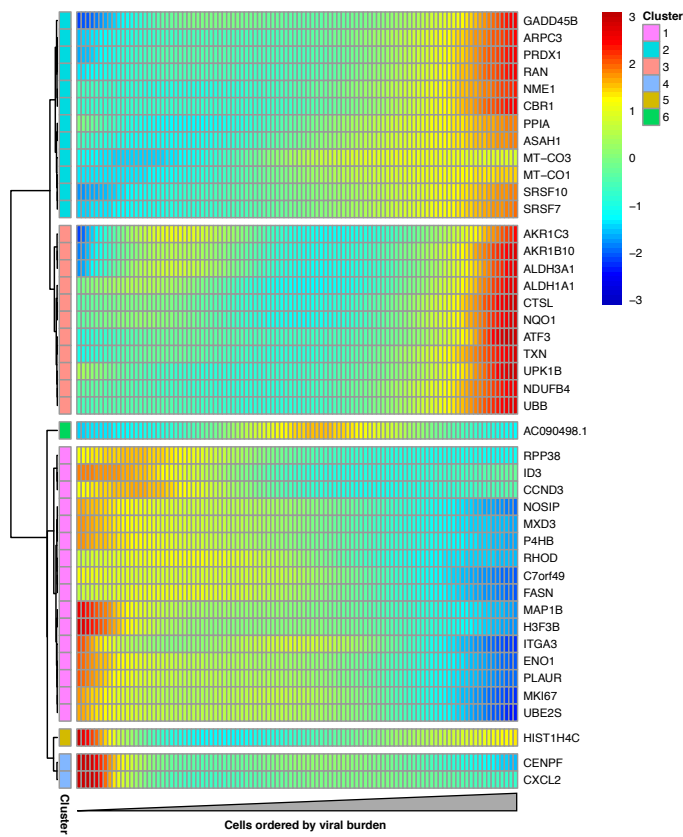


**Figure 9.** Cellular genes that co-vary in expression with the amount of viral mRNA in cells expressing all eight viral genes. The columns are cells, ordered from left to right by the fraction of mRNA derived from virus. Each row is a gene that is differentially expressed as a function of the fraction of mRNA derived from virus at a false discovery rate of 0.1. Genes for which the color goes from blue at left to red at right are expressed at higher levels in cells with more viral mRNA. The scale bar indicates the number of standard deviations above or below the mean expression, truncated at 3-fold on both sides.

**Figure 9-source data 1.** The full results of the differential expression test are in `p_sig_cellular_genes.csv`.

**Figure 9-source data 2.** A gene-set analysis for pathways associated with the amount of viral mRNA is in `p_pathway_enrichment.csv`.

**Figure 9-Figure supplement 1.** Many genes that co-vary with viral load are involved in the oxidative stress response.

**Figure 9-Figure supplement 2.** Pre-treating to reduce oxidative stress decreases the fraction of infected cells expressing detectable viral protein.

335 usually identified in genome-wide knockdown / knockout studies.

## 336 Discussion

337 We have quantified the total transcriptome composition of single cells infected with influenza virus.  
 338 While we observe a general increase in the amount of viral mRNA over time as expected from  
 339 bulk measurements (*Hatada et al., 1989; Shapiro et al., 1987*), there is wide variation in viral gene  
 340 expression among individual infected cells.

341 The most obvious form of heterogeneity is the complete failure of some infected cells to express  
 342 one or more viral genes, which we estimate occurs in about half the infected cells in our experiments.  
 343 The absence of some viral genes in some infected cells has been noted previously (*Brooke et al.,  
 344 2013; Heldt et al., 2015; Dou et al., 2017*), and our work provides a holistic view by quantifying the  
 345 total viral transcriptional load as a function of the level of each mRNA. We find that cells lacking

346 expression of any of the four genes that encode the viral RNP express much less total viral mRNA,  
 347 consistent with prior bulk studies (*Vreede et al., 2004; Eisfeld et al., 2015*). Interestingly, the reason  
 348 some cells fail to express some viral genes remains unclear. The prototypical influenza virion  
 349 packages one copy of each of the eight gene segments (*Noda et al., 2006; Hutchinson et al., 2010*),  
 350 but some virions surely package fewer (*Brooke et al., 2014*). However, it is also possible that much  
 351 of the viral gene absence is due to stochastic loss of viral RNPs after infection but prior to the  
 352 initiation of viral transcription in the nucleus.

353 The absence of viral genes only partially explains the cell-to-cell variation in amount of viral  
 354 mRNA, which still varies from <1% to >50% among cells expressing all the viral genes. It is likely  
 355 that other viral genetic factors explain some of this remaining heterogeneity. The 3'-end sequencing  
 356 strategy used in our experiments detects the presence of a viral gene, but does not identify  
 357 whether that gene contains a mutation that might hinder viral replication. However, viral mutations  
 358 are also unlikely to explain all the observed heterogeneity, since current consensus estimates of  
 359 influenza virus's mutation rate suggest that the typical virion in a stock such as the one used in our  
 360 experiment should contain less than one mutation per genome (*Parvin et al., 1986; Suárez et al.,  
 361 1992; Suárez-López and Ortín, 1994; Nobusawa and Sato, 2006; Bloom, 2014; Pauly et al., 2017*).

362 The rest of the heterogeneity must be due to some combination of cellular factors and inherent  
 363 stochasticity. Some features of the cellular transcriptome co-vary with the amount of influenza  
 364 mRNA. In particular, the viral load in individual cells is associated with the expression of genes  
 365 involved in response to cellular stresses, including oxidative stress. It will be interesting to determine  
 366 if these cellular transcriptional signatures are simply a consequence of the stress imposed by viral  
 367 replication, or if their stronger activation in some cells is a causative factor that promotes viral  
 368 transcription. However, it also would not be surprising if a substantial amount of the cell-to-cell  
 369 heterogeneity cannot be ascribed to pre-existing features of either the viral genome or cellular state.  
 370 Apparently stochastic heterogeneity is a common feature of many processes at a single-cell level (*Cai  
 371 et al., 2006; Raj et al., 2006; Buganim et al., 2012; Shalek et al., 2013; Avraham et al., 2015*) –  
 372 especially when those processes are initiated by very small numbers of initial molecules (*Elowitz  
 373 et al., 2002*), as is the case for low-MOI viral infection.

374 Our data do suggest that the factors driving the heterogeneity in viral transcriptional load exert  
 375 relatively concordant effects on all viral genes in a given cell. Specifically, despite the extreme  
 376 heterogeneity in total viral mRNA per cell, the relative levels of the viral mRNAs are reasonably  
 377 consistent across cells, and generally reflective of classical bulk measurements (*Hatada et al., 1989*).  
 378 Therefore, despite the stochasticity inherent in initiating transcription and replication of each gene  
 379 from a single copy carried by the incoming virion, as long as a gene is not completely lost then the  
 380 virus possesses mechanisms to control its relative expression (*Shapiro et al., 1987; Hatada et al.,  
 381 1989; Perez et al., 2010; Heldt et al., 2012; Chua et al., 2013*).

382 One factor that surprisingly does *not* appreciably contribute to the heterogeneity in our ex-  
 383 periments is activation of innate-immune interferon pathways. Only one of the hundreds of  
 384 virus-infected cells expresses any detectable interferon, despite the fact that a number of cells fail  
 385 to express the influenza-virus interferon antagonist NS1. It is known that interferon activation is  
 386 stochastic at the level of single cells in response to both synthetic ligands (*Shalek et al., 2013, 2014;  
 387 Bhushal et al., 2017; Hagai et al., 2017*) and actual infection (*Rand et al., 2012; Perez-Cidoncha  
 388 et al., 2014; Avraham et al., 2015; Killip et al., 2017*). But interferon expression is a prominent  
 389 transcriptional signature of high-MOI influenza virus infection of bulk cells, including in the epithelial  
 390 cell line and at the time-points used in our experiments (*Geiss et al., 2002; Sutejo et al., 2012*). So  
 391 it is notable how rarely single cells express interferon. Interferon expression would surely be more  
 392 common at later times or with a viral stock passaged at higher MOI, since paracrine interferon  
 393 signaling (*Crotta et al., 2013*) and accumulation of defective viral particles enhance innate-immune  
 394 detection (*Tapia et al., 2013; Lopez, 2014*). However, the early events of physiological influenza  
 395 infection involve just a few virions (*Varble et al., 2014; McCrone et al., 2017*), and so it is interesting  
 396 to speculate whether rare events such as interferon activation during the first few cycles of viral

397 replication could contribute to heterogeneity in the eventual outcome of infection.

398 Overall, our work shows the power and importance of characterizing cellular infection at the  
 399 level of single cells (*Avraham et al., 2015*). Viral infection can involve heterogeneity in the genetic  
 400 composition of the incoming virion, the host-cell state, the bi-modality of innate-immune activation,  
 401 and the inherent stochasticity of molecular processes initiated by a single copy of each viral gene.  
 402 In our experiments with short-timeframe and low-MOI infections with a relatively pure stock of  
 403 influenza virus, we find only a minor role for innate-immune activation, but a substantial role  
 404 for heterogeneity in the complement of viral genes that are expressed in individual cells and at  
 405 least some contribution of host-cell state. Our current experiments are not able to quantify the  
 406 role of other possibly important factors such as mutations in viral genes, but we suspect that  
 407 they may also contribute. Future extensions of the approaches described here should enable  
 408 further deconstruction of the sources of cell-to-cell heterogeneity during viral infection, thereby  
 409 enabling a deeper understanding of how the bulk features of infection emerge from processes  
 410 within individual virus-infected cells.

## 411 Methods and Materials

### 412 Cell lines and viruses

413 The following cell lines were used in this study: the human lung epithelial carcinoma line A549 (ATCC  
 414 CCL-185), the MDCK-SIAT1 variant of the Madin Darby canine kidney cell line overexpressing human  
 415 SIAT1 (Sigma-Aldrich 05071502), and the human embryonic kidney cell line 293T (ATCC CRL-3216).  
 416 The A549 cells were tested as negative for mycoplasma contamination by the Fred Hutch Genomics  
 417 Core, and authenticated using the ATCC STR profiling service. All cells were maintained in D10  
 418 media (DMEM supplemented with 10% heat-inactivated fetal bovine serum, 2 mM L-glutamine, 100  
 419 U of penicillin/ml, and 100 µg of streptomycin/ml) at 37 °C at 5 % CO<sub>2</sub>.

420 Wildtype A/WSN/1933 (H1N1) influenza virus was generated by reverse genetics using the  
 421 plasmids pHW181-PB2, pHW182-PB1, pHW183-PA, pHW184-HA, pHW185-NP, pHW186-NA, pHW187-  
 422 M, and pHW188-NS (*Hoffmann et al., 2000*). The sequences of the viral RNAs encoded in these  
 423 plasmids are in *Figure 1*-source data 1. Reverse-genetics plasmids encoding the synonymously  
 424 barcoded WSN virus were created by using site-directed mutagenesis to introduce two synonymous  
 425 mutations near the 3' end of the mRNA for each viral gene. The sequences of the synonymously  
 426 barcoded viral RNAs are in *Figure 1*-source data 1.

427 To generate viruses from these plasmids, we transfected an equimolar mix of all eight plasmids  
 428 into cocultures of 293T and MDCK-SIAT1 cells seeded at a ratio of 8:1. At 24 hours post-transfection,  
 429 we changed media from D10 to influenza growth media (Opti-MEM supplemented with 0.01% heat-  
 430 inactivated FBS, 0.3% BSA, 100 U of penicillin/ml, 100 µg of streptomycin/ml, and 100 µg of calcium  
 431 chloride/ml). At 48 hours post-transfection we harvested the virus-containing supernatant, pelleted  
 432 cellular material by centrifugation at 300 x g's for 4 minutes, and stored aliquots of the clarified  
 433 viral supernatant at -80 °C. We then titered thawed aliquots of viral by TCID50 on MDCK-SIAT1 cells,  
 434 computing titers via the formula of *Reed and Muench (1938)*. To generate our "high-purity" stocks  
 435 of viruses for the single-cell sequencing experiments, we then infected MDCK-SIAT1 cells at an MOI  
 436 of 0.01, and let the virus grow for 36 hours prior to harvesting aliquots that were again clarified by  
 437 low-speed centrifugation, aliquoted, stored at -80 °C, and titered by TCID50. The high-MOI passage  
 438 (high-defective particle) stock used in *Figure 2* was generated by instead passaging in MDCK-SIAT1  
 439 cells twice at an MOI of 1 for 48 hours.

440 For the experiments in *Figure 7-Figure Supplement 1*, we created a virus that carried an HA gene  
 441 segment in which GFP replaced most of the HA coding sequence, following a scheme first described  
 442 by *Marsh et al. (2007)*. Briefly, we created a plasmid encoding a viral RNA with GFP in place of the  
 443 HA coding sequence in the context of the pH21 (*Neumann et al., 1999*) reverse-genetics plasmid,  
 444 removing potential start codons upstream of the GFP (see *Figure 7*-source data 2 for the sequence  
 445 of the viral RNA). We then generated GFP-carrying virus by reverse-genetics in cells constitutively

446 expressing HA (*Doud and Bloom, 2016*). To obtain sufficient titers, this HA-eGFP virus was expanded  
 447 for 44 rather than 36 hours after initiating infection at an MOI of 0.01.

448 **qPCR**

449 For the qPCR in *Figure 2* and *Figure 5–Figure Supplement 1*, A549 cells were seeded at  $3 \times 10^5$   
 450 cells per well in a 6-well tissue culture plate in D10 the day prior to infection. On the day of  
 451 infection, a single well was trypsinized and the cells were counted in order to determine the  
 452 appropriate amount of virus to use to achieve the intended MOI. Immediately before infection,  
 453 D10 was replaced with influenza growth media. For cells incubated with cyclohexamide, the  
 454 compound was added to a final concentration of 50 µg/ml at the time of infection – previously  
 455 confirmed to be sufficient to halt viral protein production (*Killip et al., 2014*). RNA was purified  
 456 using the QIAGEN RNeasy plus mini kit following manufacturer's instructions. cDNA was syn-  
 457 thethesized using an oligoDT primer and the SuperScript™ III first-strand synthesis supermix from  
 458 ThermoFisher using the manufacturer's protocol. Transcript abundance was measured using  
 459 SYBR™ green PCR master mix, using a combined anneal/extension step of 60 °C for one minute  
 460 with the following primers: *HA*: 5'-GGCCCAACCACACATTCAAC-3', 5'-GCTCATCACTGCTAGACGGG-  
 461 3', *IFNB1*: 5'-AAACTCATGAGCAGTCTGCA-3', 5'-AGGAGATCTTCAGTTCGGAGG-3', *L32*: 5'-  
 462 AGCTCCCCAAAATAGACGCAC-3', 5'-TTCATAGCAGTAGGCACAAAGG-3'. Biological triplicates were per-  
 463 formed for all samples.

464 For the measurements of viral genomic HA content in *Figure 2A*, vRNA was harvested from 80  
 465 µl of viral supernatant by the addition of 600 µl of RLT plus before proceeding with the standard  
 466 QIAGEN RNeasy Plus Mini kit protocol. The cDNA was generated using SuperScript™ III first-strand  
 467 synthesis supermix using the manufacturer's protocol, and using the universal vRNA primers of  
 468 *Hoffmann et al. (2001)* with the modifications described in *Xue et al. (2017)*. The qPCR was then  
 469 performed as for mRNA measurements. A standard curve was generated from three independent  
 470 dilutions of the HA-encoding reverse genetics plasmid. All vRNA values represent three independent  
 471 RNA extractions with two replicate qPCR measurements.

472 **Flow cytometry titering and analyses**

473 To determine viral titers in terms of HA-expressing units and for the flow cytometry, A549 cells  
 474 were seeded in a 6-well plate and infected as described above for the qPCR analyses. Cells were  
 475 harvested by trypsinization, resuspended in phosphate-buffered saline supplemented with 2% heat-  
 476 inactivated FBS, and stained with 10 µg/ml of H17-L19, a mouse monoclonal antibody confirmed  
 477 to bind to WSN HA in a prior study (*Doud et al., 2017*). After washing in PBS supplemented with  
 478 2% FBS, the cells were stained with a goat anti-mouse IgG antibody conjugated to APC. Cells were  
 479 then washed, fixed in 1% formaldehyde, and washed further before a final resuspension and  
 480 analysis. We then determined the fraction of cells that were HA positive and calculated the HA-  
 481 expressing units. For NS1 staining, cells stained for HA as described above were permeabilized using  
 482 BD Cytofix/Cytoperm following manufacturer's instructions, stained with anti-NS1 (GTX125990,  
 483 Genetex) at 4.4 µg/ml, washed, stained with a goat anti-rabbit IgG antibody conjugated to Alexa  
 484 Fluor 405, washed, and analyzed. To analyze the effect of N-acetylcysteine, the compound was  
 485 added to cells in D10 9h prior to media change and infection, and included in infection media.  
 486 Stocks of N-acetylcysteine were reconstituted immediately prior to use, and the pH of growth media  
 487 supplemented with this compound was adjusted using sodium hydroxide. After channels were  
 488 compensated and cells gated to exclude multiplets and debris in FlowJo, data were extracted using  
 489 the R package flowCore (*Le Meur et al., 2007*) and analyzed using a custom Python script. Gaussian  
 490 kernel density estimates were obtained using the scipy stats package method, gaussian\_kde, using  
 491 automatic bandwidth determination (*van der Walt et al., 2017*). For gating on NS1 positive cells, the  
 492 percentage of influenza-infected cells was determined by HA staining alone, and the top quantile of  
 493 NS1-stained cells matching that percentage were taken as the NS1 positive population.

494 **Infections for single-cell mRNA sequencing**

495 Single-cell sequencing libraries were generated using the 10x Chromium Single Cell 3' plat-  
496 form ([Zheng et al., 2017](#)) using the V1 reagents.

497 All time points except for the second 8-hour sample (8hr-2) were prepared on the same day.  
498 For the infections, A549 cells were seeded in a 6-well plate, with two wells per time point. A single  
499 well of cells was trypsinized and counted prior to initiation of the experiment for the purposes of  
500 calculating MOI. Wild-type and synonymously barcoded virus were mixed to an estimated ratio  
501 of 1:1 based on prior, exploratory, single-cell analyses (data not shown). At the initiation of our  
502 experiment, the wells for all time points were changed from D10 to influenza growth media. Cells  
503 were then infected with 0.3 HA-expressing units of virus per cell (a determined by flow cytometry).  
504 The infections were performed in order of time point: first the 10-hour time point, then the  
505 8-hour, and then the 6-hour time point. At one hour after infection, the media for each time  
506 point was changed to fresh influenza growth media. Note that the HA-expressing units were  
507 calculated without this additional washing step, and so likely represent an overestimate of our  
508 final infectious dose (consistent with the fact that fewer than 30% of cells appear infected in the  
509 single-cell sequencing data). All cells were then harvested for single-cell analysis concurrently –  
510 ensuring all had spent equivalent time in changed media . For 8hr-2 sample, cells were infected  
511 as above except that the cells were infected at 0.1 HA-expressing units of virus per cell but no  
512 wash step was performed, and the sample was prepared on a different day. After harvest, cells  
513 were counted using disposable hemocytometers and diluted to equivalent concentrations with an  
514 intended capture of 3000 cells/sample following the manufacturer's provided by 10x Genomics for  
515 the Chromium Single Cell platform. All subsequent steps through library preparation followed the  
516 manufacturer's protocol. Samples were sequenced on an Illumina HiSeq.

517 **Computational analysis of single-cell mRNA sequencing data**

518 Jupyter notebooks that perform all of the computational analyses are available in Supplemen-  
519 tary file 1 and at [https://github.com/jbloomlab/flu\\_single\\_cell](https://github.com/jbloomlab/flu_single_cell) ([Russell et al., 2018](#), copy archived at  
520 [https://github.com/elife sciences-publications/flu\\_single\\_cell](https://github.com/elife sciences-publications/flu_single_cell)).

521 Briefly, the raw deep sequencing data were processed using the 10X Genomics software pack-  
522 age CellRanger (version 2.0.0). The reads were aligned to a concatenation of the human and  
523 influenza virus transcriptomes. The human transcriptome was generated by filtering genome  
524 assembly GRCh38 for protein coding genes defined in the GTF file GRCh38.87. The influenza  
525 virus transcriptome was generated from the reverse-complement of the wildtype WSN viral  
526 RNA sequences as encoded in the reverse-genetics plasmids ([Figure 1](#)-source data 1). The  
527 aligned deep sequencing data are available on the GEO repository under accession GSE108041  
528 (<https://www.ncbi.nlm.nih.gov/geo/query/acc.cgi?acc=GSE108041>).

529 CellRanger calls cells based on the number of observed cell barcodes, and creates a cell-gene  
530 matrix. We used custom Python code to annotate the cells in this matrix by the number of viral  
531 reads that could be assigned to the wildtype and synonymously barcoded virus. Only about half of  
532 the viral reads overlapped the barcoded regions of the genes ([Figure 1A](#)) and could therefore be  
533 assigned to a viral barcode ([Figure 4-Figure Supplement 1](#)). So for calculations of the number of  
534 reads in a cell derived from each viral barcode for each viral gene, the total number of detected  
535 molecules of that gene are multiplied by the fraction of those molecules with assignable barcodes  
536 that are assigned to that barcode. This annotated cell-gene matrix is in Supplementary file 2. A  
537 Jupyter notebook that performs these analyses is in Supplementary file 1.

538 The annotated cell-gene matrix was analyzed in R, primarily using the Monocle package (version  
539 2.4.0) ([Qiu et al., 2017; Trapnell et al., 2014](#)). A Jupyter notebook that performs these analyses is in  
540 Supplementary file 1. For each sample, cell barcodes that had >2.5-fold fewer or more UMI counts  
541 mapping to cellular transcripts than the sample mean were excluded from downstream analyses  
542 (see red vertical lines in [Figure 3B](#)).

543 In order to determine an appropriate cutoff for how many reads a cell needed to contain in

order to be classified as infected, we calculated the mean viral barcode purity across all cells that contained at least a given fraction of viral mRNA and had multiple viral reads that could be assigned a barcode (**Figure 4B,C** and **Figure 4–Figure Supplement 2**). We then determined the threshold fraction of viral mRNA at which the mean purity no longer increased as a function of the amount of viral mRNA. This threshold represents the point at which we have effectively eliminated cells that have low barcode purity simply due to lysis-acquired reads sampled randomly from both viral barcodes. As is apparent from **Figure 4B**, only the 10-hour sample and the 8hr-2 sample have the excess of mixed barcodes among cells with low amounts of viral mRNA. The likely reason is that these samples have more total viral mRNA (and so there is more available mRNA to be acquired from lysed cells); in addition, there is always some experimental variability in the amount of cell lysis during the 10X sequencing process, and these samples may simply have the most. So the above threshold procedure is appropriate for those two samples. For the other samples, we simply set a minimum threshold of requiring at least a fraction  $2 \times 10^{-4}$  reads to come from viral mRNA as explained in the legend to **Figure 4–Figure Supplement 2**. The thresholds for each sample are shown in **Figure 4C** and **Figure 4–Figure Supplement 2**. This procedure is expected to be conservative, and may miss some truly infected cells with very low amounts of viral mRNA. For subsequent analyses, we retained all infected cells and a subsample of uninfected cells (the greater of 50 or the number of infected cells for that sample). The rationale for subsampling the uninfected cell is that the vast majority of cells are uninfected, and we did not want these cells to completely dominate the downstream analyses. Cells were classified as co-infected if both viral variants had an RNA level that exceeded the threshold, and if the minor variant contributed at least 5% of the viral mRNA.

For the semi-supervised t-SNE clustering, we used Monocle's cell hierarchy function to bin cells into those with no viral mRNA, <2% viral mRNA, between 2% and 20% viral mRNA, and >20%. Candidate marker genes for t-SNE dimensionality reduction were then determined using the Monocle function `markerDiffTable`, excluding the effects of sample variation and the number of genes identified in a given cell, using a q-value cutoff of 0.01. The specificity of these markers was determined using the function `calculateMarkerSpecificity` – the top 50 markers were retained, and used to place populations in a two-dimensional plane based on tSNE dimensionality reduction.

For the analyses of cellular genes that differed in expression as a function of the amount of viral mRNA, we only considered cells that expressed all 8 viral mRNAs to avoid effects driven simply by viral gene absence. We also only considered cellular genes in the differential gene analysis, since viral gene expression will tautologically co-vary with the amount of viral mRNA. Additionally, because influenza virus has the capacity to degrade or prevent the synthesis of host mRNAs (*Bercovich-Kinori et al., 2016*) and contributes significantly to the total number UMIs in some cells, we calculate size factors (a scalar value representing efficiency of UMI capture) based on cellular transcripts alone. Finally, we assigned all cells a ceiling fraction of mRNA from virus of 25% so that a few extremely high-expressing cells did not dominate. Cellular genes with expression that co-varied with the fraction of viral mRNAs in a cell were then determined using the Monocle `differentialGeneTest`, after removing variance explained by sample to sample variation. **Figure 9** shows all genes that were significantly associated with the fraction of mRNA from virus at a false discovery rate of 0.1. We performed the gene set analysis using the P -values from the Monocle `differentialGeneTest` with *piano* (*Väremo et al., 2013*) using the hallmark gene set from GSEA v6 (*Subramanian et al., 2005*) and Fisher's method.

## 588 Acknowledgments

589 We thank Xiaojie Qiu for advice about use of the Monocle software package, David Bacsik and  
 590 Robert Bradley for comments on the manuscript, and the Fred Hutch Genomics Core for performing  
 591 the Illumina deep sequencing.

## 592      References

- 593      **Aguilera ER**, Erickson AK, Jesudhasan PR, Robinson CM, Pfeiffer JK. Plaques formed by mutagenized viral  
594      populations have elevated coinfection frequencies. *mBio*. 2017; 8(2):e02020.
- 595      **Akpınar F**, Timm A, Yin J. High-Throughput Single-Cell Kinetics of Virus Infections in the Presence of Defective  
596      Interfering Particles. *Journal of Virology*. 2016 Jan; 90(3):1599–1612.
- 597      **Alvaredo F**. A note on the relationship between top income shares and the Gini coefficient. *Economics Letters*.  
598      2011; 110(3):274–277.
- 599      **Amatore D**, Sgarbanti R, Aquilano K, Baldelli S, Limongi D, Civitelli L, Nencioni L, Garaci E, Ciriolo MR, Palamara  
600      AT. Influenza virus replication in lung epithelial cells depends on redox-sensitive pathways activated by  
601      NOX4-derived ROS. *Cellular microbiology*. 2014 Oct; 17(1):131–145.
- 602      **Avraham R**, Haseley N, Brown D, Penaranda C, Jijon HB, Trombetta JJ, Satija R, Shalek AK, Xavier RJ, Regev A, et al.  
603      Pathogen cell-to-cell variability drives heterogeneity in host immune responses. *Cell*. 2015; 162(6):1309–1321.
- 604      **Banning A**, Deubel S, Kluth D, Zhou Z, Brigelius-Flohe R. The GI-GPx Gene Is a Target for Nrf2. *Molecular and  
605      Cellular Biology*. 2005 May; 25(12):4914–4923.
- 606      **Bercovich-Kinori A**, Tai J, Gelbart IA, Shitrit A, Ben-Moshe S, Drori Y, Itzkovitz S, Mandelboim M, Stern-Ginossar  
607      N. A systematic view on influenza induced host shutoff. *eLife*. 2016 Aug; 5:e18311.
- 608      **Bhushal S**, Wolfsmüller M, Selvakumar TA, Kemper L, Wirth D, Hornef MW, Hauser H, Köster M. Cell polarization  
609      and epigenetic status shape the heterogeneous response to Type III interferons in intestinal epithelial cells.  
610      *Frontiers in immunology*. 2017; 8:671.
- 611      **Bloom JD**. An experimentally determined evolutionary model dramatically improves phylogenetic fit. *Molecular  
612      Biology and Evolution*. 2014; 31(8):1956–1978.
- 613      **Brooke CB**, Ince WL, Wrammert J, Wrammert J, Ahmed R, Wilson PC, Bennink JR, Yewdell JW. Most Influenza A  
614      Virions Fail To Express at Least One Essential Viral Protein. *Journal of Virology*. 2013 Feb; 87(6):3155–3162.
- 615      **Brooke CB**. Biological activities of ‘noninfectious’ influenza A virus particles. *Future Virology*. 2014 Jan; 9(1):41–51.
- 616      **Brooke CB**, Ince WL, Wei J, Bennink JR, Yewdell JW. Influenza A virus nucleoprotein selectively decreases  
617      neuraminidase gene-segment packaging while enhancing viral fitness and transmissibility. *Proceedings of  
618      the National Academy of Sciences*. 2014; 111(47):16854–16859.
- 619      **Buganim Y**, Faddah DA, Cheng AW, Itsikovich E, Markoulaki S, Ganz K, Klemm SL, van Oudenaarden A, Jaenisch R.  
620      Single-cell expression analyses during cellular reprogramming reveal an early stochastic and a late hierachic  
621      phase. *Cell*. 2012; 150(6):1209–1222.
- 622      **Cai L**, Friedman N, Xie XS. Stochastic protein expression in individual cells at the single molecule level. *Nature*.  
623      2006; 440(7082):358–362.
- 624      **Cao J**, Packer JS, Ramani V, Cusanovich DA, Huynh C, Daza R, Qiu X, Lee C, Furlan SN, Steemers FJ, et al.  
625      Comprehensive single-cell transcriptional profiling of a multicellular organism. *Science*. 2017; 357(6352):661–  
626      667.
- 627      **Chen S**, Chen S, Short JAL, Young DF, Killip MJ, Schneider M, Schneider M, Goodbourn S, Randall RE. Heterocellular  
628      induction of interferon by negative-sense RNA viruses. *Virology*. 2010 Nov; 407(2):247–255.
- 629      **Chua MA**, Schmid S, Perez JT, Langlois RA, et al. Influenza A virus utilizes suboptimal splicing to coordinate the  
630      timing of infection. *Cell reports*. 2013; 3(1):23–29.
- 631      **Combe M**, Garijo R, Geller R, Cuevas JM, Sanjuán R. Single-cell analysis of RNA virus infection identifies multiple  
632      genetically diverse viral genomes within single infectious units. *Cell host & microbe*. 2015; 18(4):424–432.
- 633      **Crotta S**, Davidson S, Mahlakoiv T, Desmet CJ, Buckwalter MR, Albert ML, Staeheli P, Wack A. Type I and type III  
634      interferons drive redundant amplification loops to induce a transcriptional signature in influenza-infected  
635      airway epithelia. *PLoS Pathogens*. 2013; 9(11):e1003773.
- 636      **Dapat C**, Saito R, Suzuki H, Horigome T. Quantitative phosphoproteomic analysis of host responses in human  
637      lung epithelial (A549) cells during influenza virus infection. *Virus research*. 2014 Jan; 179:53–63.

- 638    **Delbruck M.** The burst size distribution in the growth of bacterial viruses (bacteriophages). *Journal of bacteriology*. 1945 Aug; 50(2):131–135.
- 640    **Dimmock NJ**, Dimmock NJ, Easton AJ, Easton AJ. Defective Interfering Influenza Virus RNAs: Time To Reevaluate  
641    Their Clinical Potential as Broad-Spectrum Antivirals? *Journal of Virology*. 2014 Apr; 88(10):5217–5227.
- 642    **Dou D**, Hernández-Neuta I, Wang H, Östbye H, Qian X, Thiele S, Resa-Infante P, Kouassi NM, Sender V, Henrich K,  
643    Mellroth P, Henriques-Normark B, Gabriel G, Nilsson M, Daniels R. Analysis of IAV Replication and Co-infection  
644    Dynamics by a Versatile RNA Viral Genome Labeling Method. *Cell reports*. 2017 Jul; 20(1):251–263.
- 645    **Doud M**, Bloom J. Accurate Measurement of the Effects of All Amino-Acid Mutations on Influenza Hemagglutinin.  
646    *Viruses*. 2016 Jun; 8(6):155–17.
- 647    **Doud MB**, Hensley SE, Bloom JD. Complete mapping of viral escape from neutralizing antibodies. *PLoS Pathogens*. 2017 Mar; 13(3):e1006271.
- 649    **Doyle V**, Virji S, Crompton M. Evidence that cyclophilin-A protects cells against oxidative stress. *The Biochemical journal*. 1999 Jul; 341 ( Pt 1)(Pt 1):127–132.
- 651    **Dubois J**, Terrier O, Rosa-Calatrava M. Influenza viruses and mRNA splicing: doing more with less. *MBio*. 2014;  
652    5(3):e00070–14.
- 653    **Duong HQ**, You K, Oh S, Kwak SJ, Seong YS. Silencing of NRF2 Reduces the Expression of ALDH1A1 and ALDH3A1  
654    and Sensitizes to 5-FU in Pancreatic Cancer Cells. *Antioxidants*. 2017 Sep; 6(3):52–10.
- 655    **Eisfeld AJ**, Neumann G, Kawaoka Y. At the centre: influenza A virus ribonucleoproteins. *Nature reviews Microbiology*. 2015; 13(1):28.
- 657    **Elowitz MB**, Levine AJ, Siggia ED, Swain PS. Stochastic gene expression in a single cell. *Science*. 2002;  
658    297(5584):1183–1186.
- 659    **Fensterl V**, Sen GC. The ISG56/IFIT1 gene family. *Journal of Interferon & Cytokine Research*. 2011 Jan; 31(1):71–  
660    78.
- 661    **Fonville JM**, Marshall N, Tao H, Steel J, Lowen AC. Influenza Virus Reassortment Is Enhanced by Semi-  
662    infectious Particles but Can Be Suppressed by Defective Interfering Particles. *PLoS Pathogens*. 2015 Oct;  
663    11(10):e1005204.
- 664    **García-Sastre A**, Egorov A, Matassov D, Brandt S, Levy DE, Durbin JE, Palese P, Muster T. Influenza A virus lacking  
665    the NS1 gene replicates in interferon-deficient systems. *Virology*. 1998; 252(2):324–330.
- 666    **Geiss GK**, Salvatore M, Tumpey TM, Carter VS, Wang X, Basler CF, Taubenberger JK, Bumgarner RE, Palese P, Katze MG, García-Sastre A. Cellular transcriptional profiling in influenza A virus-infected lung epithelial cells: the role of the nonstructural NS1 protein in the evasion of the host innate defense and its potential contribution to pandemic influenza. *Proceedings of the National Academy of Sciences of the United States of America*. 2002 Aug; 99(16):10736–10741.
- 671    **Gini C.** Measurement of inequality of incomes. *The Economic Journal*. 1921; 31(121):124–126.
- 672    **Gorrini C**, Harris IS, Mak TW. Modulation of oxidative stress as an anticancer strategy. *Nature Publishing Group*.  
673    2013 Dec; 12(12):931–947.
- 674    **Hagai T**, Chen X, Miragaia RJ, Gomes T, Rostom R, Kunowska N, Proserpio V, Donati G, Bossini-Castillo L, Naamati G, Emerton G, Trynka G, Kondova I, Denis M, Teichmann SA. Gene expression variability across cells and species shapes innate immunity. *bioRxiv*. 2017; doi: 10.1101/137992.
- 677    **Hale BG**, Randall RE, Ortín J, Jackson D. The multifunctional NS1 protein of influenza A viruses. *Journal of General Virology*. 2008; 89(10):2359–2376.
- 679    **Hatada E**, Hasegawa M, Mukaigawa J, Shimizu K, Fukuda R. Control of influenza virus gene expression: quantitative analysis of each viral RNA species in infected cells. *The Journal of Biochemistry*. 1989; 105(4):537–546.
- 681    **Heldt FS**, Frensing T, Reichl U. Modeling the intracellular dynamics of influenza virus replication to understand  
682    the control of viral RNA synthesis. *Journal of Virology*. 2012; 86(15):7806–7817.
- 683    **Heldt FS**, Kupke SY, Dorl S, Reichl U, Frensing T. Single-cell analysis and stochastic modelling unveil large  
684    cell-to-cell variability in influenza A virus infection. *Nature communications*. 2015 Nov; 6:1–12.

- 685 **Hoffmann E**, Stech J, Guan Y, Webster RG, Perez DR. Universal primer set for the full-length amplification of all  
686 influenza A viruses. *Archives of virology*. 2001 Dec; 146(12):2275–2289.
- 687 **Hoffmann E**, Neumann G, Kawaoka Y, Hobom G, Webster RG. A DNA transfection system for generation of  
688 influenza A virus from eight plasmids. *Proceedings of the National Academy of Sciences*. 2000; 97(11):6108–  
689 6113.
- 690 **Huang AS**, Baltimore D, et al. Defective viral particles and viral disease processes. *Nature*, London. 1970;  
691 226:325–7.
- 692 **Huang IC**, Li W, Sui J, Marasco W, Choe H, Farzan M. Influenza A Virus Neuraminidase Limits Viral Superinfection.  
693 *Journal of Virology*. 2008 Apr; 82(10):4834–4843.
- 694 **Huang T**, Palese P, Krystal M. Determination of influenza virus proteins required for genome replication. *Journal of Virology*. 1990; 64(11):5669–5673.
- 696 **Hutchinson EC**, von Kirchbach JC, Gog JR, Digard P. Genome packaging in influenza A virus. *Journal of general  
697 virology*. 2010; 91(2):313–328.
- 698 **Iwasaki A**, Pillai PS. Innate immunity to influenza virus infection. *Nature Reviews Immunology*. 2014 May;  
699 14(5):315–328.
- 700 **Jiang X**, An Z, Lu C, Chen Y, Du E, Qi S, Yang K, Zhang Z, Xu Y. The protective role of Nrf2-Gadd45b against  
701 antimony-induced oxidative stress and apoptosis in HEK293 cells. *Toxicology Letters*. 2016 Aug; 256:11–18.
- 702 **Jung KA**, Lee S, Kwak MK. NFE2L2/NRF2 Activity Is Linked to Mitochondria and AMP-Activated Protein Kinase Signaling in Cancers Through miR-181c/Mitochondria-Encoded Cytochrome C Oxidase Regulation. *Antioxidants & Redox Signaling*. 2017 Apr; p. ars.2016.6797–3.
- 705 **Kallfass C**, Lienenklaus S, Weiss S, Staeheli P. Visualizing the beta interferon response in mice during infection with influenza A viruses expressing or lacking nonstructural protein 1. *Journal of Virology*. 2013 Jun;  
706 87(12):6925–6930.
- 708 **Killip MJ**, Jackson D, Perez-Cidoncha M, Fodor E, Randall RE. Single-cell studies of IFN- $\beta$  promoter activation by  
709 wild-type and NS1-defective influenza A viruses. *Journal of General Virology*. 2017 Mar; 98(3):357–363.
- 710 **Killip MJ**, Smith M, Jackson D, Randall RE. Activation of the Interferon Induction Cascade by Influenza A Viruses  
711 Requires Viral RNA Synthesis and Nuclear Export. *Journal of Virology*. 2014 Mar; 88(8):3942–3952.
- 712 **Killip MJ**, Fodor E, Randall RE. Influenza virus activation of the interferon system. *Virus research*. 2015 Feb; .
- 713 **Kim KH**, Jeong JY, Surh YJ, Kim KW. Expression of stress-response ATF3 is mediated by Nrf2 in astrocytes. *Nucleic  
714 Acids Research*. 2009 Oct; 38(1):48–59.
- 715 **Klein AM**, Mazutis L, Akartuna I, Tallapragada N, Veres A, Li V, Peshkin L, Weitz DA, Kirschner MW. Droplet  
716 Barcoding for Single-Cell Transcriptomics Applied to Embryonic Stem Cells. *Cell*. 2015 May; 161(5):1187–1201.
- 717 **Lauring AS**, Andino R. Quasispecies Theory and the Behavior of RNA Viruses. *PLoS Pathogens*. 2010 Jul;  
718 6(7):e1001005–8.
- 719 **Le Meur N**, Hahne F, Ellis B, Haaland P. FlowCore: data structures package for flow cytometry data. *Bioconductor Project*; 2007.
- 721 **Lee D**, Ryu KY. Effect of cellular ubiquitin levels on the regulation of oxidative stress response and proteasome  
722 function via Nrf1. *Biochemical and Biophysical Research Communications*. 2017 Apr; 485(2):234–240.
- 723 **Leonard AS**, Weissman D, Greenbaum B, Ghedin E, Koelle K. Transmission Bottleneck Size Estimation from  
724 Pathogen Deep-Sequencing Data, with an Application to Human Influenza A Virus. *Journal of Virology*. 2017;  
725 p. JV1-00171–17.
- 726 **Lin X**, Wang R, Zou W, Sun X, Liu X, Zhao L, Wang S, Jin M. The Influenza Virus H5N1 Infection Can Induce ROS  
727 Production for Viral Replication and Host Cell Death in A549 Cells Modulated by Human Cu/Zn Superoxide  
728 Dismutase (SOD1) Overexpression. *Viruses*. 2016 Jan; 8(1):13–16.
- 729 **Lopez CB**. Defective Viral Genomes: Critical Danger Signals of Viral Infections. *Journal of Virology*. 2014 Jul;  
730 88(16):8720–8723.

- 731   **Van der Maaten L**, Hinton G. Visualizing data using t-SNE. *Journal of Machine Learning Research*. 2008; 9:2579–2605.
- 733   **MacLeod AK**, Acosta-Jimenez L, Coates PJ, McMahon M, Carey FA, Honda T, Henderson CJ, Wolf CR. Aldo-keto  
734   reductases are biomarkers of NRF2 activity and are co-ordinately overexpressed in non-small cell lung cancer.  
735   *British journal of cancer*. 2016 Dec; 115(12):1530–1539.
- 736   **Macosko EZ**, Basu A, Satija R, Nemesh J, Shekhar K, Goldman M, Tirosh I, Bialas AR, Kamitaki N, Martersteck EM,  
737   et al. Highly parallel genome-wide expression profiling of individual cells using nanoliter droplets. *Cell*. 2015;  
738   161(5):1202–1214.
- 739   **von Magnus P**. Incomplete forms of influenza virus. *Advances in Virus Research*. 1954; 2:59–79.
- 740   **Marsh GA**, Hatami R, Palese P. Specific residues of the influenza A virus hemagglutinin viral RNA are important  
741   for efficient packaging into budding virions. *Journal of Virology*. 2007; 81(18):9727–9736.
- 742   **McCrone JT**, Woods RJ, Martin ET, Malosh RE, Monto AS, Lauring AS. Stochastic processes dominate the within  
743   and between host evolution of influenza virus. *bioRxiv*. 2017; p. 176362.
- 744   **Miura T**, Taketomi A, Nishinaka T, Terada T. Regulation of human carbonyl reductase 1 (CBR1, SDR21C1) gene  
745   by transcription factor Nrf2. *Chemico-Biological Interactions*. 2013 Feb; 202(1-3):126–135.
- 746   **Murray J**, Taylor SW, Zhang B, Ghosh SS, Capaldi RA. Oxidative Damage to Mitochondrial Complex I Due to  
747   Peroxynitrite. *Journal of Biological Chemistry*. 2003 Sep; 278(39):37223–37230.
- 748   **Neumann G**, Watanabe T, Ito H, Watanabe S, Goto H, Gao P, Hughes M, Perez DR, Donis R, Hoffmann E, Hobom  
749   G, Kawaoka Y. Generation of influenza A viruses entirely from cloned cDNAs. *Proceedings of the National  
750   Academy of Sciences of the United States of America*. 1999 Aug; 96(16):9345–9350.
- 751   **Nobusawa E**, Sato K. Comparison of the mutation rates of human influenza A and B viruses. *Journal of Virology*.  
752   2006; 80(7):3675–3678.
- 753   **Noda T**, Sagara H, Yen A, Takada A, Kida H, Cheng RH, Kawaoka Y. Architecture of ribonucleoprotein complexes  
754   in influenza A virus particles. *Nature*. 2006; 439(7075):490.
- 755   **Parvin JD**, Moscona A, Pan W, Leider J, Palese P. Measurement of the mutation rates of animal viruses: influenza  
756   A virus and poliovirus type 1. *Journal of Virology*. 1986; 59(2):377–383.
- 757   **Pauly MD**, Procario MC, Lauring AS. A novel twelve class fluctuation test reveals higher than expected mutation  
758   rates for influenza A viruses. *eLife*. 2017; 6:e26437.
- 759   **Perez JT**, Varble A, Sachidanandam R, Zlatev I, Manoharan M, García-Sastre A, et al. Influenza A virus-generated  
760   small RNAs regulate the switch from transcription to replication. *Proceedings of the National Academy of  
761   Sciences*. 2010; 107(25):11525–11530.
- 762   **Perez-Cidoncha M**, Killip MJ, Oliveros JC, Asensio VJ, Fernandez Y, Bengoechea JA, Randall RE, Ortín J. An  
763   Unbiased Genetic Screen Reveals the Polygenic Nature of the Influenza Virus Anti-Interferon Response.  
764   *Journal of Virology*. 2014 Apr; 88(9):4632–4646.
- 765   **Peuchant E**, Bats ML, Moranvillier I, Lepoivre M, Guittot J, Wendum D, Lacombe ML, Moreau-Gaudry F, Boissan  
766   M, Dabernat S. Metastasis suppressor NM23 limits oxidative stress in mammals by preventing activation of  
767   stress-activated protein kinases/JNKs through its nucleoside diphosphate kinase activity. *The FASEB Journal*.  
768   2017 Mar; 31(4):1531–1546.
- 769   **Poon LL**, Song T, Rosenfeld R, Lin X, Rogers MB, Zhou B, Sebra R, Halpin RA, Guan Y, Twaddle A, DePasse JV,  
770   Stockwell TB, Wentworth DE, Holmes EC, Greenbaum B, Peiris JSM, Cowling BJ, Ghedin E. Quantifying influenza  
771   virus diversity and transmission in humans. *Nature Genetics*. 2016; 48(2):195–200.
- 772   **Qiu X**, Mao Q, Tang Y, Wang L, Chawla R, Pliner HA, Trapnell C. Reversed graph embedding resolves complex  
773   single-cell trajectories. *Nature Methods*. 2017 Aug; p. 1–10.
- 774   **Raj A**, Peskin CS, Tranchina D, Vargas DY, Tyagi S. Stochastic mRNA synthesis in mammalian cells. *PLoS Biology*.  
775   2006; 4(10):e309.
- 776   **Rand U**, Rinas M, Schwerk J, Nöhren G, Linné M, Kröger A, Flossdorf M, Kullai KK, Hauser H, Höfer T, Köster M.  
777   Multi-layered stochasticity and paracrine signal propagation shape the type-I interferon response. *Molecular  
778   Systems Biology*. 2012 Jan; 8(1):584.

- 779    **Reed LJ**, Muench H. A simple method of estimating fifty percent endpoints. *American journal of epidemiology*.  
 780    1938; 27(3):493–497.
- 781    **Russell AB**, Trapnell C, Bloom JD. Computer code for “Extreme heterogeneity of influenza virus infection in  
 782    single cells”. Github. 2018; commit ce72599. [https://github.com/jbloomlab/flu\\_single\\_cell](https://github.com/jbloomlab/flu_single_cell).
- 783    **Saira K**, Lin X, DePasse JV, Halpin R, Twaddle A, Stockwell T, Angus B, Cozzi-Lepri A, Delfino M, Dugan V, Dwyer  
 784    DE, Freiberg M, Horban A, Losso M, Lynfield R, Wentworth DN, Holmes EC, Davey R, Wentworth DE, Ghedin E.  
 785    Sequence analysis of in vivo defective interfering-like RNA of influenza A H1N1 pandemic virus. *Journal of  
 786    Virology*. 2013; 87(14):8064–8074.
- 787    **Schulte MB**, Andino R. Single-Cell Analysis Uncovers Extensive Biological Noise in Poliovirus Replication. *Journal  
 788    of Virology*. 2014 May; 88(11):6205–6212.
- 789    **Sgarbanti R**, Amatore D, Celestino I, Marcocci ME, Fraternale A, Ciriolo MR, Magnani M, Saladino R, Garaci E,  
 790    Palamara AT, Nencioni L. Intracellular redox state as target for anti-influenza therapy: are antioxidants always  
 791    effective? *Current topics in medicinal chemistry*. 2014; 14(22):2529–2541.
- 792    **Shalek AK**, Satija R, Adiconis X, Gertner RS, Gaublomme JT, Raychowdhury R, Schwartz S, Yosef N, Malboeuf C,  
 793    Lu D, et al. Single-cell transcriptomics reveals bimodality in expression and splicing in immune cells. *Nature*.  
 794    2013; 498(7453):236–241.
- 795    **Shalek AK**, Satija R, Shuga J, Trombetta JJ, Gennert D, Lu D, Chen P, Gertner RS, Gaublomme JT, Yosef N, et al.  
 796    Single cell RNA Seq reveals dynamic paracrine control of cellular variation. *Nature*. 2014; 510(7505):363.
- 797    **Shapiro GI**, Gurney T, Krug RM. Influenza virus gene expression: control mechanisms at early and late times of  
 798    infection and nuclear-cytoplasmic transport of virus-specific RNAs. *Journal of Virology*. 1987 Mar; 61(3):764–  
 799    773.
- 800    **Suárez P**, Valcarcel J, Ortín J. Heterogeneity of the mutation rates of influenza A viruses: isolation of mutator  
 801    mutants. *Journal of Virology*. 1992; 66(4):2491–2494.
- 802    **Suárez-López P**, Ortín J. An estimation of the nucleotide substitution rate at defined positions in the influenza  
 803    virus haemagglutinin gene. *Journal of general virology*. 1994; 75(2):389–393.
- 804    **Subramanian A**, Tamayo P, Mootha VK, Mukherjee S, Ebert BL, Gillette MA, Paulovich A, Pomeroy SL, Golub TR,  
 805    Lander ES, et al. Gene set enrichment analysis: a knowledge-based approach for interpreting genome-wide  
 806    expression profiles. *Proceedings of the National Academy of Sciences*. 2005; 102(43):15545–15550.
- 807    **Sutejo R**, Yeo DS, Zu Myaing M, Hui C, Xia J, Ko D, Cheung PC, Tan BH, Sugrue RJ. Activation of Type I and III  
 808    Interferon Signalling Pathways Occurs in Lung Epithelial Cells Infected with Low Pathogenic Avian Influenza  
 809    Viruses. *PLoS ONE*. 2012; 7(3).
- 810    **Tapia K**, Kim Wk, Sun Y, Mercado-López X, Dunay E, Wise M, Adu M, López CB. Defective viral genomes arising  
 811    in vivo provide critical danger signals for the triggering of lung antiviral immunity. *PLoS Pathogens*. 2013;  
 812    9(10):e1003703.
- 813    **Trapnell C**, Cacchiarelli D, Grimsby J, Pokharel P, Li S, Morse M, Lennon NJ, Livak KJ, Mikkelsen TS, Rinn JL. The  
 814    dynamics and regulators of cell fate decisions are revealed by pseudotemporal ordering of single cells. *Nature  
 815    Biotechnology*. 2014 Mar; 32(4):381–386.
- 816    **Varble A**, Albrecht RA, Backes S, Crumiller M, Bouvier NM, Sachs D, García-Sastre A, et al. Influenza A virus  
 817    transmission bottlenecks are defined by infection route and recipient host. *Cell host & microbe*. 2014;  
 818    16(5):691–700.
- 819    **Väremo L**, Nielsen J, Nookaei I. Enriching the gene set analysis of genome-wide data by incorporating  
 820    directionality of gene expression and combining statistical hypotheses and methods. *Nucleic Acids Research*.  
 821    2013; 41(8):4378–4391.
- 822    **Vreede FT**, Jung TE, Brownlee GG. Model Suggesting that Replication of Influenza Virus Is Regulated by  
 823    Stabilization of Replicative Intermediates. *Journal of Virology*. 2004 Aug; 78(17):9568–9572.
- 824    **van der Walt S**, Colbert SC, Varoquaux G. The NumPy Array: A Structure for Efficient Numerical Computation.  
 825    *Computing in Science & Engineering*. 2017 Aug; 13(2):22–30.
- 826    **Watanabe T**, Watanabe S, Kawaoka Y. Cellular networks involved in the influenza virus life cycle. *Cell Host &  
 827    Microbe*. 2010; 7(6):427–439.

- 828    **Xue J**, Chambers BS, Hensley SE, López CB. Propagation and Characterization of Influenza Virus Stocks That  
829       Lack High Levels of Defective Viral Genomes and Hemagglutinin Mutations. *Frontiers in microbiology*. 2016  
830       Mar; 7(Pt 10):e1004924–15.
- 831    **Xue KS**, Stevens-Ayers T, Campbell AP, Englund JA, Pergam SA, Boeckh M, Bloom JD. Parallel evolution of  
832       influenza across multiple spatiotemporal scales. *eLife*. 2017 Jun; 6:e26875.
- 833    **Zheng GX**, Terry JM, Belgrader P, Ryvkin P, Bent ZW, Wilson R, Ziraldo SB, Wheeler TD, McDermott GP, Zhu J, et al.  
834       Massively parallel digital transcriptional profiling of single cells. *Nature communications*. 2017; 8:14049.
- 835    **Zhu Y**, Yongky A, Yin J. Growth of an RNA virus in single cells reveals a broad fitness distribution. *Virology*. 2009;  
836       385(1):39–46.

**Supplementary file 1.** Computer code for the analyses. This ZIP file contains a Jupyter notebook that runs CellRanger to align and annotate the reads, and a Jupyter notebook that uses Monocle to analyze the cell-gene matrix. The ZIP file also includes associated custom scripts. To just run the Monocle analysis in `monocle_analysis.ipynb` on a pre-generated cell-gene matrix, unpack Supplementary file 2 into `./results/cellgenecounts/`.

**Supplementary file 2.** The annotated cell-gene matrix in Matrix Market Format. This is the matrix generated in `./results/cellgenecounts/` by running the CellRanger analysis in `align_and_annotate.ipynb` in Supplementary file 1. This file is available on DataDryad at <https://doi.org/10.5061/dryad.qp0t3>.

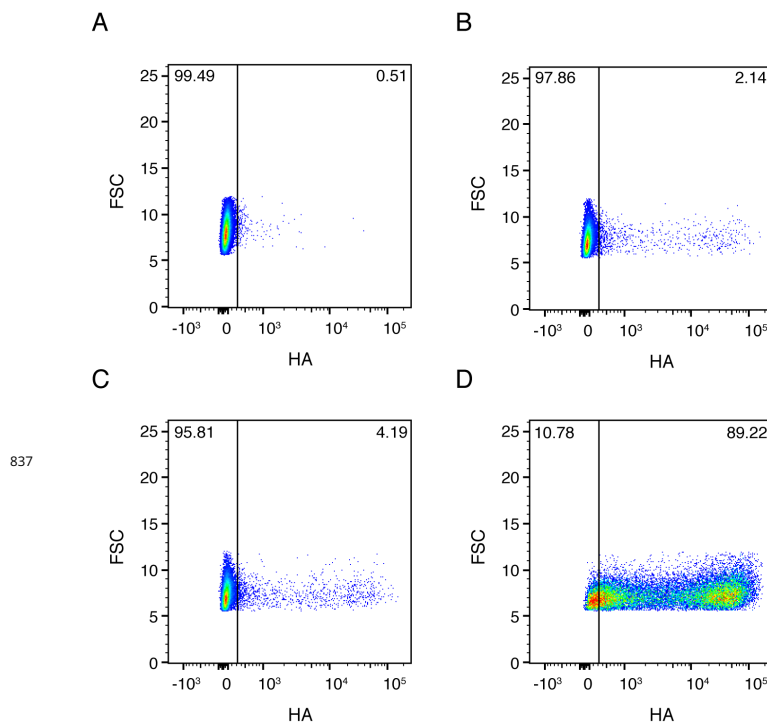


**Figure 2–Figure supplement 1.** Full flow cytometry data for Figure 2B. A549 cells were infected at an MOI of 0.1 as calculated by TCID<sub>50</sub> on MDCK-SIAT1 cells. **(A)** Uninfected gating control. **(B)** Cells infected with the wild-type virus stock used in our experiments. **(C)** Cells infected with synonymously barcoded virus stock used in our experiments. **(D)** Cells infected with a stock of wild-type virus propagated at a high MOI, and therefore enriched in defective particles.

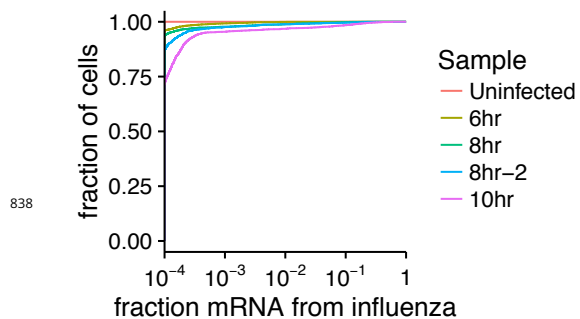


**Figure 3–Figure supplement 1.** For each sample, this plot shows the fraction of all cells that derive at least the indication fraction of their mRNA from influenza virus.

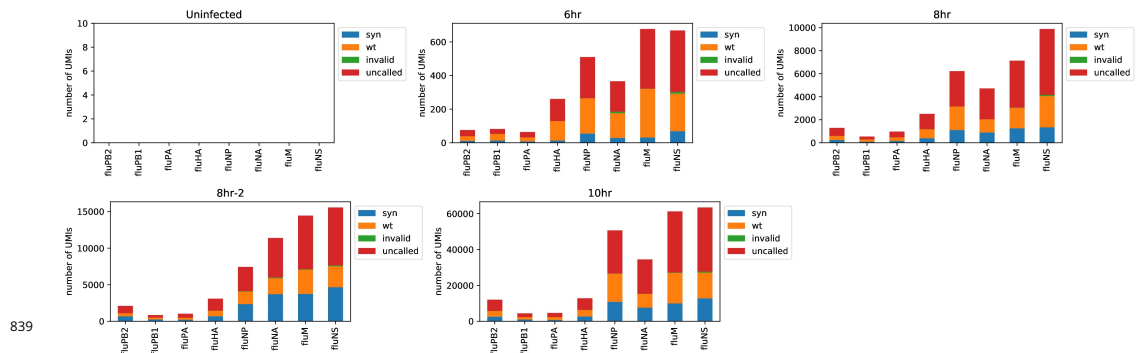


**Figure 4-Figure supplement 1.** The number of viral barcodes called for each sample and gene segment. Viral transcripts are classified as *syn* if they mapped to a synonymously barcoded influenza transcript, *wt* if they mapped to a wild-type influenza transcript, *invalid* if multiple reads for the same UMI differed on the status of the viral barcode, and as *uncalled* if none of the reads for that UMI overlapped the region of the viral transcript containing the viral barcode. For calculations of the number of reads in a cell derived from each viral barcode for each viral gene, the total number of detected molecules of that gene are multiplied by the fraction of those molecules with assignable barcodes that are assigned to that barcode.

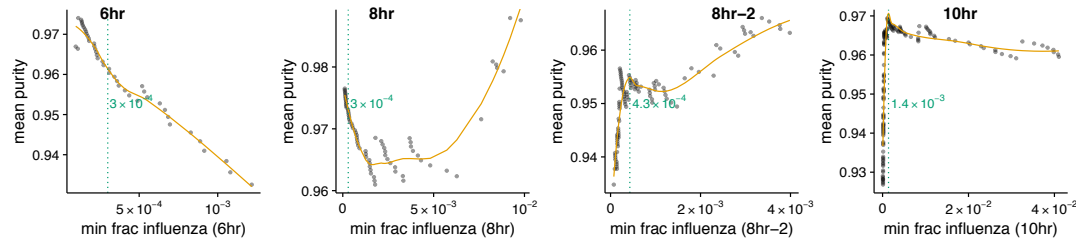


**Figure 4-Figure supplement 2.** Cell lysis can lead cells to the spurious association of small amounts of extraneous mRNA with individual cells. We wanted to avoid classifying as infected cells that had simply acquired such lysis-derived viral mRNA. The amount of lysis-derived viral mRNA will vary among samples as a function of both the lysis rate during the cell preparation (which always varies slightly from sample to sample in the 10X procedure) and with the amount of total viral mRNA for that sample (the more viral mRNA, the more there is to be acquired from lysed cells). As is shown in Figure 4B, the 8hr-2 and 10hr sample clearly have an enrichment of mixed barcodes in cells with small numbers of viral mRNA. For each sample, we calculated the mean purity of all cells with at least the indicated amount of viral mRNA, and determined the threshold amount of viral mRNA where purity no longer increased by finding the first maxima in a loess curve fit (orange line). We called the threshold at this point of maximum purity (dotted green line). For the 6hr and 8hr samples there is no indication of contamination from lysis-derived reads, as Figure 4B shows no increase in mixed barcodes in low viral mRNA cells. Therefore, for these samples we simply set a threshold of requiring at least  $2 \times 10^{-4}$  of the total mRNA to come from virus, which corresponds to  $\sim 2$  viral mRNAs for the typical cell with  $10^4$  total reads (Figure 3B).

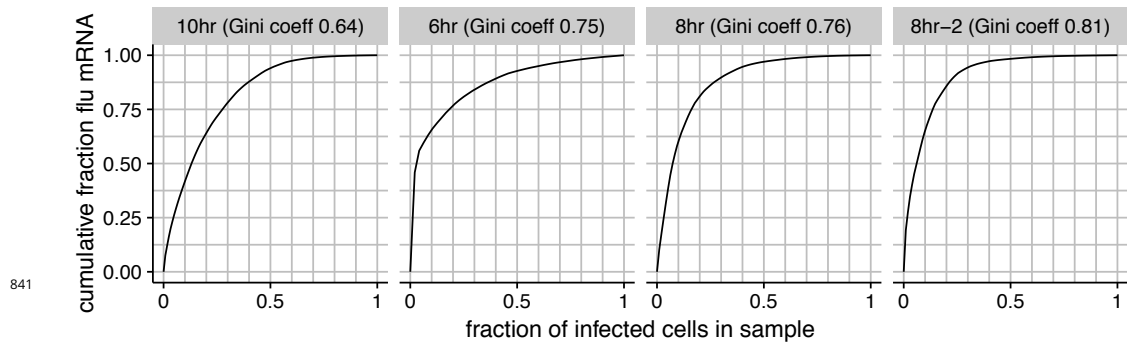


**Figure 4-Figure supplement 3.** The total fraction of all viral mRNA among infected cells that is attributable to a given fraction of these cells. For instance, the plot for the 8hrs sample shows that ~50% of all viral mRNA is derived from ~8% of the infected cells. The facet titles above each plot also give the Gini coefficient ([Gini, 1921](#)) that calculates the heterogeneity in the distribution of viral mRNA among infected cells. Gini coefficients of 0 indicate a perfectly even distribution across cells, and Gini coefficients of 1 indicate a maximally skewed distribution.

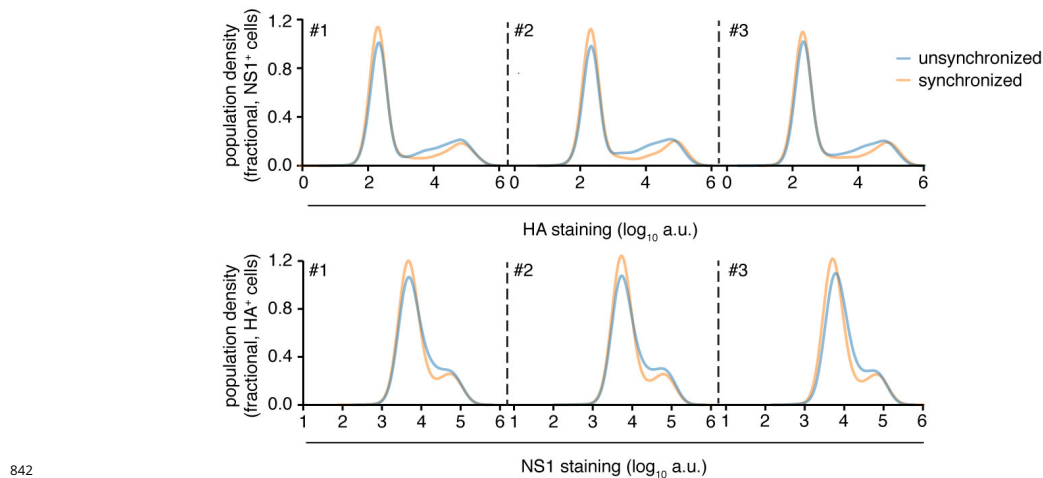


**Figure 4-Figure supplement 4.** Flow cytometry analysis of expression of viral proteins in cells infected at an MOI of 0.1 (unsynchronized) or 0.2 (synchronized) as calculated by TCID50 on MDCK-SIAT1 cells. The higher MOI for synchronized infections was to attempt to account for loss of virus in washing steps. Infections were synchronized by pre-adsorbing virus at 4°C for 1h prior to initiation of infection by shifting temperature to 37°C using pre-warmed media. Cells were concurrently stained for HA and NS1 proteins at 10 hours after initiation of infection, and then analyzed by flow cytometry. The level of HA protein was quantified in cells that were identified as infected based on being positive for NS1 protein (top), and the level of NS1 protein was quantified in cells that were identified as infected based on being positive for HA protein (bottom). Synchronization resulted in a small decrease in variability in the levels of each viral protein, particularly in cells with intermediate levels. But the effects were small compared to the overall variability in the protein levels, indicating timing of infection makes only a small contribution to the observed heterogeneity. Data are shown for three independent replicates.

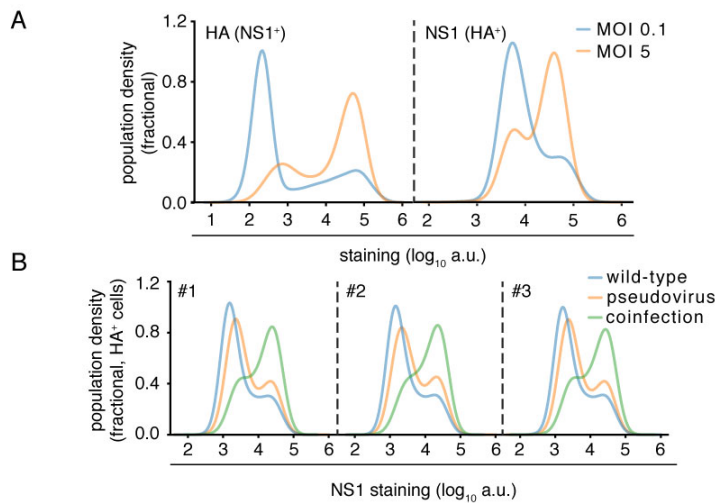


**Figure 4-Figure supplement 5. (A)** Flow cytometry analysis of expression of viral proteins in cells infected at high (MOI 5 as calculated by TCID50 on MDCK-SIAT1 cells) or low (MOI 0.1) initial infectious dose. Cells were concurrently stained for HA and NS1 proteins at 10 hours after initiation of infection, and then analyzed by flow cytometry. The level of HA protein was quantified in cells that were identified as infected based on being positive for NS1 protein (left), and the level of NS1 protein was quantified in cells that were identified as infected based on being positive for HA protein (right). While a higher dose leads to more cells expressing high amounts of viral protein, it does not greatly increase the amount of viral protein in either the low-expressing or high-expressing cells. Therefore, higher viral dose does not lead to a large continuous increase in viral protein production among all cells – rather, it mostly changes the proportions of cells that fall in different parts of the highly heterogeneous distribution. **(B)** Cells were co-infected with a mix of wild-type virus and pseudovirus in which the HA gene was replaced by GFP flanked by the terminal regions of the HA gene segment at an MOI of 0.1 for each virus. At 10 hours post-infection, cells were stained for NS1 and HA expression and analyzed by flow cytometry for these proteins and GFP. Cells could be annotated as infected by virions of the same type (wild-type infection indicated by presence of HA, or pseudovirus infection indicated by the presence of GFP) or both types of virions (indicated by presence of HA and GFP). Coinfected cells, like cells infected at a higher infectious dose, occupy different positions in the distribution of viral protein production but do not exhibit a continuous increase in viral protein production. Data are shown for three independent replicates.

843

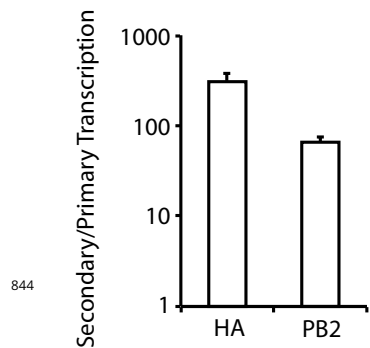


**Figure 5–Figure supplement 1.** A549 cells were infected at an MOI of 0.2 as calculated on MDCK-SIAT1 cells in either the presence or absence of the protein-translation inhibitor cyclohexamide, and viral mRNA was quantified at 8 hours post-infection by qPCR. The cyclohexamide prevents translation of new PB2, PB1, PA, and NP protein, and so prevents the formation of the new RNPs needed for secondary transcription. The bars show the relative amount of HA and PB2 mRNA in the absence versus the presence of cyclohexamide. Error  $\pm$  S.D. n=3.

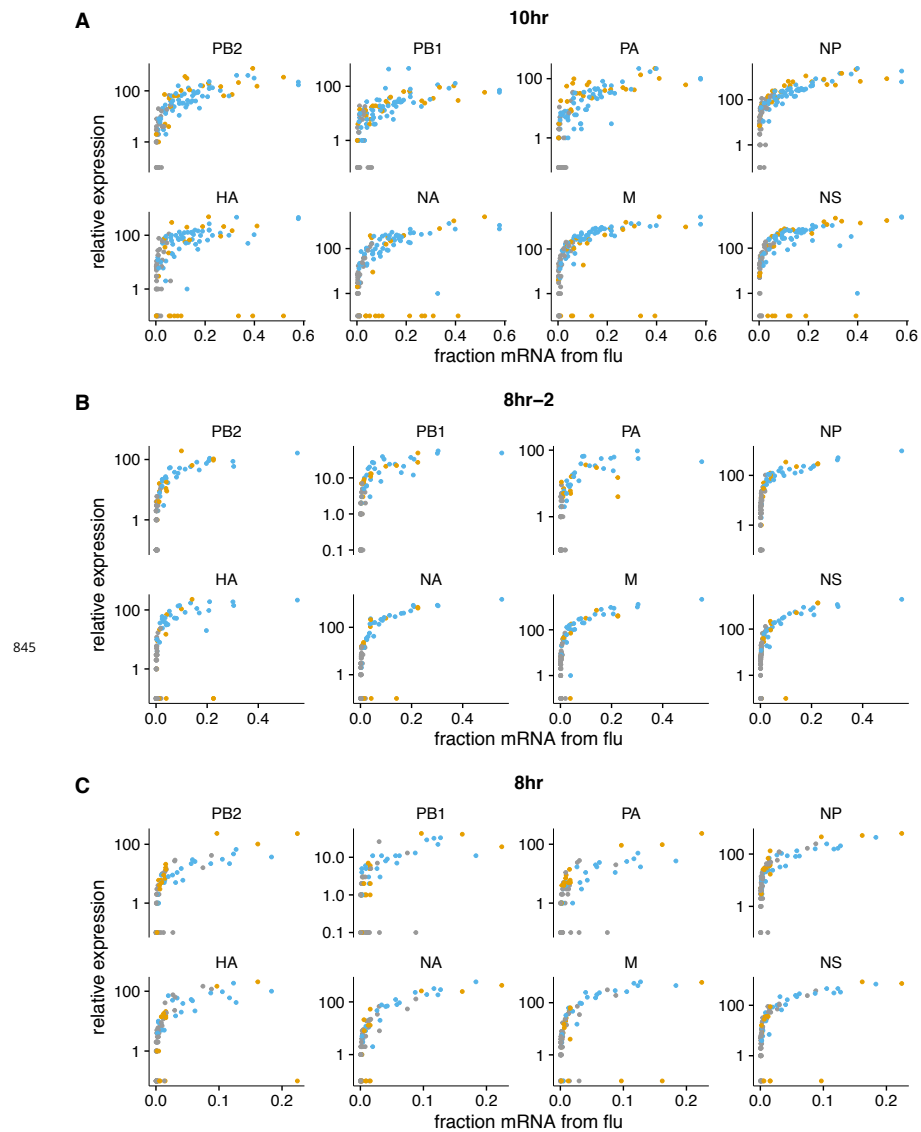


**Figure 5–Figure supplement 2.** The normalized expression of each viral gene as a function of the fraction of total mRNA derived from virus, shown for the 10-hour and 8-hour samples individually (the other samples had too few infected cells for this analysis to be useful). Points are colored as in **Figure 5A**.

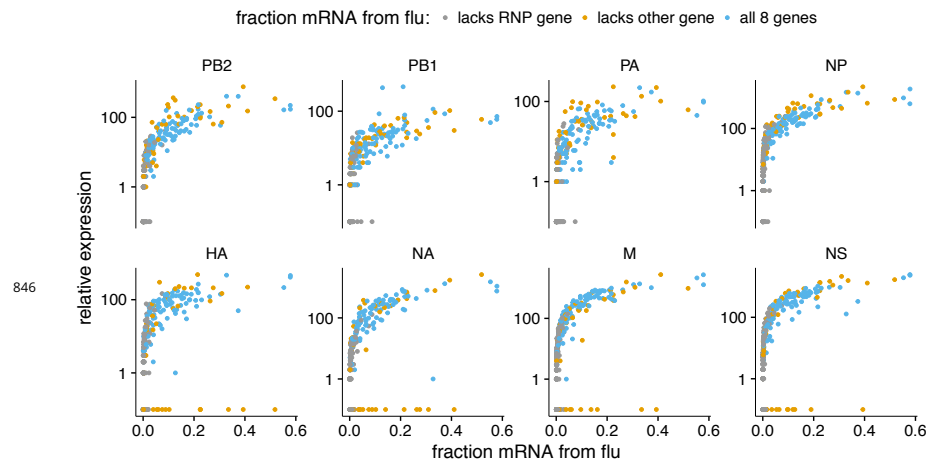


**Figure 5-Figure supplement 3.** The normalized expression of each viral gene as a function of the fraction of total mRNA derived from virus, excluding cells that were annotated as coinfected based on the presence of both viral barcodes.

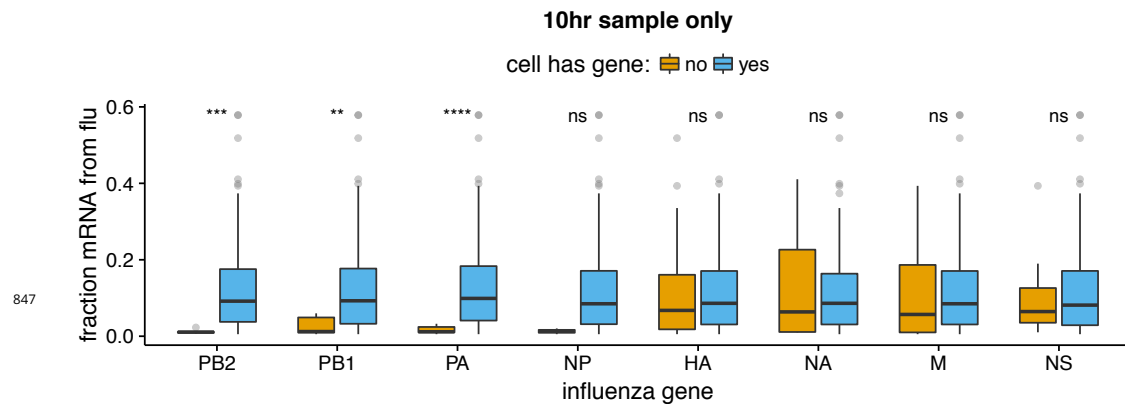


**Figure 5-Figure supplement 4.** The absence of viral RNP genes but *not* non-RNP genes remains significantly associated with reduced viral burden when we examine only the 10-hr sample, which is the single time point with the most data points. The difference for NP is no longer statistically significant due to low counts of infected cells lacking NP, but the trend remains. We do not show statistical analyses for other samples, as the number of infected cells is too low.

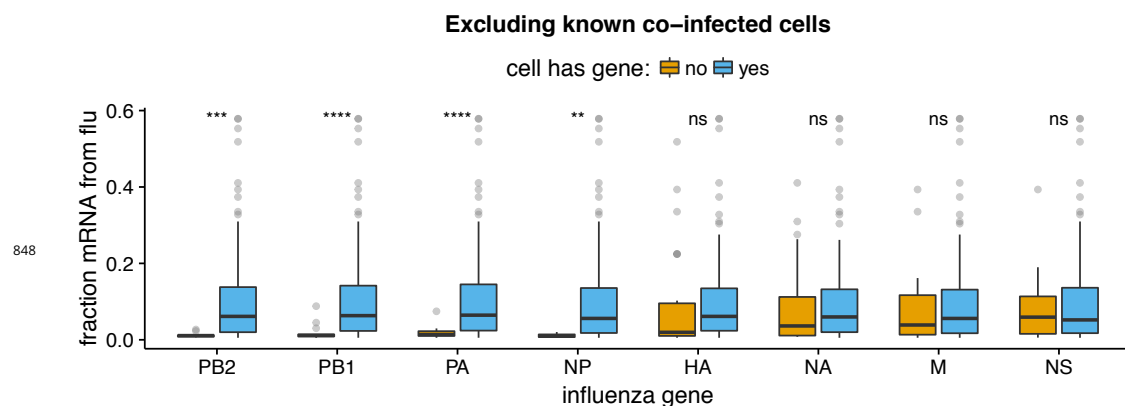


**Figure 5-Figure supplement 5.** All findings in **Figure 5B** remain unchanged if we exclude cells called as coinfecting based on the presence of mixed viral barcodes.

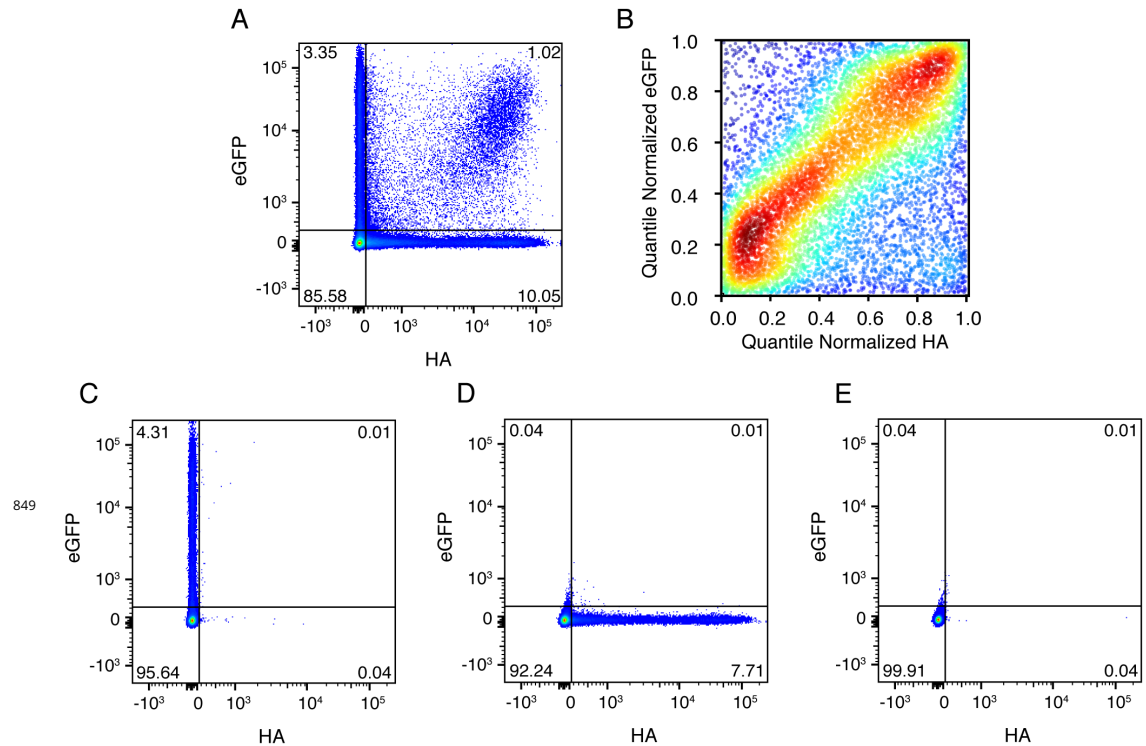


**Figure 7-Figure supplement 1.** **(A)** Cells were co-infected with a mix of wild-type virus and virus in which the HA gene was replaced by GFP flanked by the terminal regions of the HA gene segment. At 10 hours post-infection, cells were analyzed by flow cytometry for HA and eGFP expression. **(B)** The expression of HA and GFP are correlated in co-infected cells. Shown are the quantile-normalized HA and eGFP signals for double-positive cells. Cells are colored by density, using a Gaussian kernel density estimate. **(C),(D),(E)** Gating controls, single infection with eGFP virus, single infection with wild-type virus, and uninfected cells, respectively.

Category	Genes
Detoxification	AKR1C3, AKR1B10, ALDH3A1, ALDH1A1, NQO1, CBR1, PRDX1
Protein folding	TXN, PPIA
Electron transport chain	NDUFB4, MT-CO1, MT-CO3
Regulators	ATF3, GADD45B
ROS-responsive relevance complex/unknown	UBB, NME1

**Figure 9-Figure supplement 1.** Table delineating genes in Figure 9 that are associated with the response to oxidative stress (*Duong et al., 2017; Jung et al., 2017; Lee and Ryu, 2017; Peuchant et al., 2017; MacLeod et al., 2016; Jiang et al., 2016; Gorrini et al., 2013; Miura et al., 2013; Kim et al., 2009; Banning et al., 2005; Murray et al., 2003; Doyle et al., 1999*).

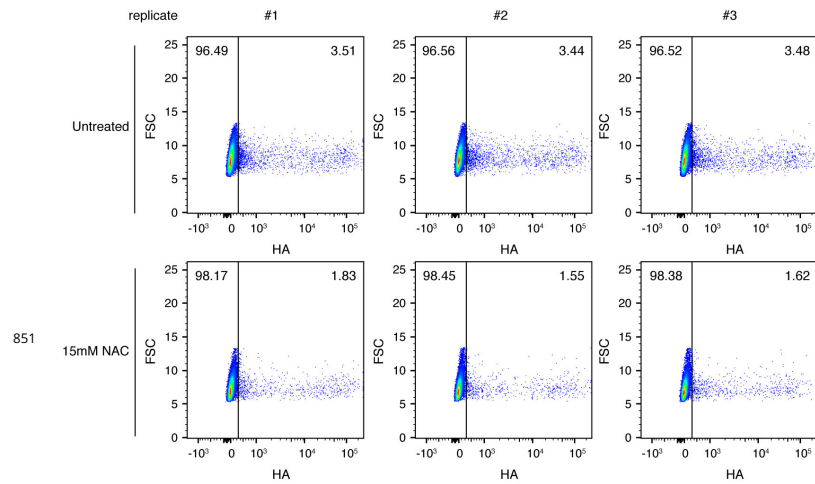


**Figure 9–Figure supplement 2.** Cells were treated as indicated with 15 mM N-acetylcysteine (NAC), an antioxidant, and infected at an MOI of 0.1 as calculated by TCID<sub>50</sub> on MDCK-SIAT1 cells. At 10 hours post-infection, cells were analyzed by flow cytometry for HA expression. The percentage of HA-positive cells is indicated on the flow cytometry plots. Data are shown for three independent replicates.